iScience

CellPress
OPEN ACCESS

Article

SARS-CoV-2 ferritin nanoparticle vaccines produce hyperimmune equine sera with broad sarbecovirus activity

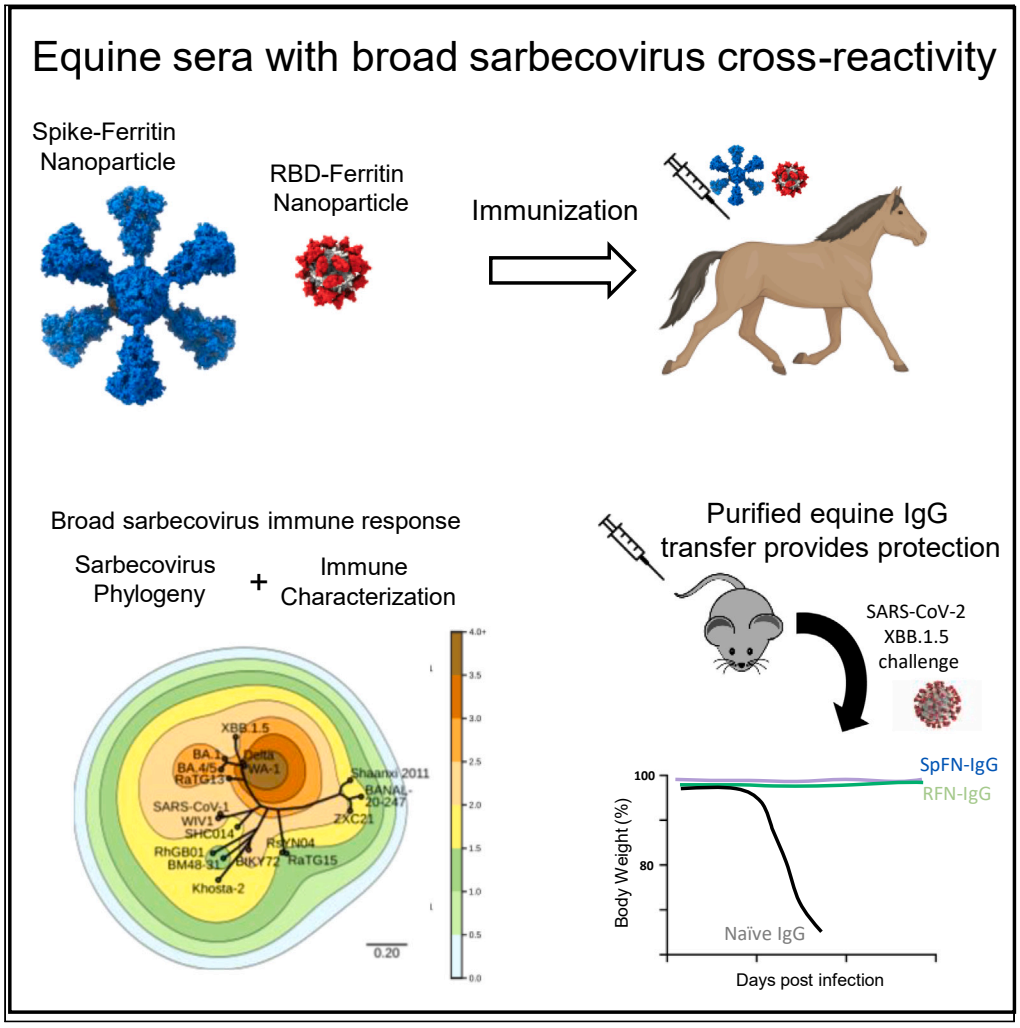

Elizabeth J. Martinez, William C. Chang, Wei-Hung Chen, ..., Kayvon Modjarrad, John Kaundinya, M. Gordon Joyce

john.k@rivaara-inc.com (J.K.)
gjoyce@eidresearch.org (M.G.J.)

Highlights

SARS-CoV-2 next-generation nanoparticle vaccines elicit hyperimmune sera in horses

Phylogenetic-contour maps illustrate sera cross-reactivity across sarbecovirus

Equine sera neutralize all tested SARS-CoV-2 VoC, and SARS-CoV-1 pseudoviruses

Purified equine IgG protected K18-hACE2 mice against SARS-CoV-2 XBB.1.5 challenge

Martinez et al., iScience 27, 110624
October 18, 2024
https://doi.org/10.1016/j.isci.2024.110624

iScience

CellPress
OPEN ACCESS

Article

SARS-CoV-2 ferritin nanoparticle vaccines produce hyperimmune equine sera with broad sarbecovirus activity

Elizabeth J. Martinez,[1,2,11,15] William C. Chang,[1,2,15] Wei-Hung Chen,[1,2] Agnes Hajduczki,[1,2] Paul V. Thomas,[1,2] Jaime L. Jensen,[1,2] Misook Choe,[1,2,12] Rajeshwer S. Sankhala,[1,2,13] Caroline E. Peterson,[1,2] Phyllis A. Rees,[1,2] Jordan Kimner,[2,3] Sandrine Soman,[3] Caitlin Kuklis,[3] Letzibeth Mendez-Rivera,[2,4] Vincent Dussupt,[2,4] Jocelyn King,[1,2] Courtney Corbett,[1,2] Sandra V. Mayer,[1,2] Aldon Fernandes,[6,9] Kripa Murzello,[7] Tres Cookenham,[7] Janine Hvizdos,[7] Larry Kummer,[7] Tricia Hart,[7] Kathleen Lanzer,[7] Julian Gambacurta,[7] Matthew Reagan,[7] Debbie Duso,[7] Sandhya Vasan,[1,2] Natalie D. Collins,[1] Nelson L. Michael,[5] Shelly J. Krebs,[4] Gregory D. Gromowski,[3] Kayvon Modjarrad,[1,14] John Kaundinya,[8,10,*] and M. Gordon Joyce[1,2,16,*]

SUMMARY

The rapid emergence of SARS-CoV-2 variants of concern (VoC) and the threat of future zoonotic sarbecovirus spillover emphasizes the need for broadly protective next-generation vaccines and therapeutics. We utilized SARS-CoV-2 spike ferritin nanoparticle (SpFN), and SARS-CoV-2 receptor binding domain ferritin nanoparticle (RFN) immunogens, in an equine model to elicit hyperimmune sera and evaluated its sarbecovirus neutralization and protection capacity. Immunized animals rapidly elicited sera with the potent neutralization of SARS-CoV-2 VoC, and SARS-CoV-1 pseudoviruses, and potent binding against receptor binding domains from sarbecovirus clades 1b, 1a, 2, 3, and 4. Purified equine polyclonal IgG provided protection against Omicron XBB.1.5 virus in the K18-hACE2 transgenic mouse model. These results suggest that SARS-CoV-2-based nanoparticle vaccines can rapidly produce a broad and protective sarbecovirus response in the equine model and that equine serum has therapeutic potential against emerging SARS-CoV-2 VoC and diverse sarbecoviruses, presenting a possible alternative or supplement to monoclonal antibody immunotherapies.

INTRODUCTION

The emergence of the COVID-19 global pandemic spurred rapid and effective development of SARS-CoV-2 vaccines and therapeutics, but the long-term need for pan-sarbecovirus and pan-coronavirus interventions persist. The concerns of the pandemic remain due to the evolution and emergence of new variants; sarbecovirus reservoirs with overlapping geographic ranges and viral lineages using hACE2 orthologues make future spillover events highly likely.[1–4] Convalescent plasma and monoclonal antibodies (mAbs) have been instrumental therapeutics among people infected with SARS-CoV-2. Immunotherapies, especially with mAbs, are highly specific and can be effective, but the time and expense needed to develop and produce them delay their rapid deployment.[5] Moreover, single mAbs have unfortunately been shown to quickly lose efficacy against emerging SARS-CoV-2 variants of concern (VoC), as mutations in the mAb epitope allow for viral escape; the

[1]Emerging Infectious Diseases Branch, Walter Reed Army Institute of Research, Silver Spring, MD, USA
[2]Henry M. Jackson Foundation for the Advancement of Military Medicine, Bethesda, MD, USA
[3]Viral Diseases Branch, Walter Reed Army Institute of Research, Silver Spring, MD, USA
[4]U.S. Military HIV Research Program, Walter Reed Army Institute of Research, Silver Spring, MD, USA
[5]Center for Infectious Diseases Research, Walter Reed Army Institute of Research, Silver Spring, MD, USA
[6]Bharat Serums and Vaccines Ltd., Mumbai, Maharashtra, India
[7]Trudeau Institute, Saranac Lake, NY, USA
[8]BSV Biosciences, Inc., Morgan Hill, CA, USA
[9]Present address: GeNei Laboratories Pvt. Ltd., Bangalore, Karnataka, India
[10]Present address: Rivaara, Inc., Carlsbad, CA, USA
[11]Present address: U of Washington, Seattle, WA 98195, USA
[12]Present address: Vaccine Research Center, NIH, Bethesda, MD 20852, USA
[13]Present address: Hansoh Bio, Rockville, MD 20850, USA
[14]Present address: Pfizer, Pearl River, NY 10965, USA
[15]These authors contributed equally
[16]Lead contact
*Correspondence: john.k@rivaara-inc.com (J.K.), gjoyce@eidresearch.org (M.G.J.)
https://doi.org/10.1016/j.isci.2024.110624

development of updated therapeutics against VoC is needed.[6–22] While the use of human convalescent plasma has shown mixed efficacy[12,17,23–29] it currently remains as one of the most important lines of defense against SARS-CoV-2 for the treatment of COVID-19 in patients with immunosuppressive disease or receiving immunosuppressive treatment. The further development of next-generation hyper-immune plasma with high neutralization potency against SARS-CoV-2 VoC represents a therapeutic option that can be readily updated upon the emergence of novel VoC and could be less susceptible compared to monoclonal antibodies to loss of efficacy due to viral immune escape.

Since their initial application in the 19th century against diphtheria, heterologous polyclonal antibodies (pAbs) have been used for the management of infections and toxin exposures.[30] Horses are most commonly used for the production of cost-effective therapeutic pAbs, given the large amounts and titer of sera available[31] – more than 10-fold less expensive than mAbs by one estimate[32] – and low- and middle-income countries (LMICs) have established facilities and capacity to produce equine plasma to fulfill needs for immunotherapeutics.[32,33] Equine sera has also been noted to have increased levels of antigen binding breadth due to the large and diverse nature of the polyclonal immune response, enabling their utility as snake venom antidote preparations.[34] Advances in serum and antibody processing have mitigated some of the adverse effects of earlier crude preparations, such as the elimination of endotoxins and removal of Fc fragments to prevent anaphylaxis[35,36]. Worldwide, heterologous polyclonal antibodies are still the only antivenom treatment against bites and stings from snakes, scorpions, and spiders,[37] and are also used to treat infections by pathogens such as rabies virus and *Clostridium tetani* in LMICs where the availability of human-derived antibodies is limited[38,39]. With their broad specificity and high titers, equine pAbs can retain effectiveness against emerging virus variants and compensate for diminished neutralization potency against a single strain. As a therapeutic, equine sera are rapidly developable and have been described for emerging infectious diseases including Middle East respiratory syndrome coronavirus (MERS-CoV), Ebola virus, and influenza virus[5,35,40]. Elicitation of SARS-CoV-2 neutralizing serum in the equine model has been described, but these examples were assessed in the context of limited VoCs, while the immunogens and immunization schedule utilized is extensive, adding significant time to the process.[41–43] Antibodies derived from plasma from another large mammal, transchromosomic bovines carrying a human immunoglobulin gene repertoire, hyperimmunized with SARS-CoV-2 spike pDNA and protein, showed the neutralization of SARS-CoV-2 variants including BA.1[44,45] and protection from mortality after challenge in hamsters[46]; phase 2 clinical trials were completed[47] but the phase 3 trial was discontinued due to low COVID-19 hospitalizations.[48]

In recent years, there have been multiple examples of engineered immunogens utilizing nanoparticle platforms to elicit improved immune responses. The *H. pylori* ferritin is a self-assembling 24-subunit molecule that can present antigens on its surface and has been used to generate enhanced immune responses. Examples include influenza hemagglutinin (HA) and HA stabilized stem, and Epstein-Barr virus (EBV) gp350 and gH/gL. These ferritin nanoparticle immunogens have progressed to phase I human clinical studies.[39–42] Our group has designed multiple SARS-CoV-2 immunogens fused to an *H. pylori* ferritin core with two lead candidates, (i) a stabilized SARS-CoV-2 Spike protein Ferritin Nanoparticle (SpFN), and (ii) a receptor binding domain (RBD) Ferritin Nanoparticle (RFN). Assessments of these immunogens in a phase 1 human clinical trial, and in murine, hamster and non-human primate immunogenicity studies showed consistently robust and broad immunogenicity, and *in vivo* protection.[49–55]

Here, we immunized horses with either SpFN or RFN to further characterize the immune response derived from each immunogen and to generate polyclonal serum with potential therapeutic capacity. We assessed the breadth and potency of the equine sera in relation to SARS-CoV-2 VoC and SARS-CoV-1 neutralization, and the binding responses against a panel of highly divergent sarbecovirus RBD molecules. We mapped these data using a novel phylogenetic tree-contour map to visualize the sarbecovirus immune response. We assessed the ability of purified polyclonal IgG from the immunized horses to protect against SARS-CoV-2 Omicron XBB.1.5 viral challenge in the K18-hACE2 transgenic murine model. The breadth and potency present in the equine polyclonal sera have implications for therapeutic interventions and pan-CoV vaccine development.

RESULTS

Spike ferritin nanoparticle and receptor binding domain ferritin nanoparticle immunization in an equine model generates hyperimmune sera with broad receptor binding domain binding capacity

We evaluated our two lead SARS-CoV-2 vaccine candidates, SpFN and RFN, in an equine model to generate hyperimmune sera and characterize the immune response in this model. SpFN and RFN (Figure 1A) were administered at two doses (500 μg or 150 μg) adjuvanted with Complete Freund's Adjuvant or Incomplete Freund's Adjuvant (CFA/IFA), in either a 3- or 4-week interval schedule (Figures 1B and Table S1). Blood was regularly drawn 1-week or 2-week following vaccination for serological analysis.

To assess the humoral immune response, sera samples following each immunization were examined by Octet biolayer interferometry (BLI) against a panel of SARS-CoV-2 RBD molecules. Both the 150 μg and 500 μg doses resulted in similar binding responses that were statistically equivalent (Figures 1C and 1D). We assessed the breadth of the immune response to SARS-CoV-2 RBD molecules from WA-1 and VoC Alpha (B.1.1.7), Beta (B.1.351), Delta (B.1.617.2), and Omicrons BA.1, BA.2, BA.4/5, BA.2.86, and XBB.1.5, and SARS-CoV-1 (Figures 1C and 1D, Tables S3–S5, and Figure S1). Initial strong binding responses of ∼ 1–2 nm were observed for WA-1, Alpha, and Delta VoC RBDs after the initial immunization of SpFN or RFN; binding was low but detectable for Beta and all Omicron variants tested. The RBD binding response elicited by RFN was in general higher than that seen for SpFN.

Following the second immunization, sera from both SpFN and RFN immunized groups showed high binding levels (>1 nm) to all VoC RBDs, with the levels remaining largely constant following the third immunization. Between the first and second timepoint, and the first and third timepoint, responses were significantly different (p-values $\leq$0.01, or $\leq$0.001 respectively) (Tables S2–S5). Similarly, antibody responses assessed by ELISA increased between the first and the second dose and remained generally constant between the second and third

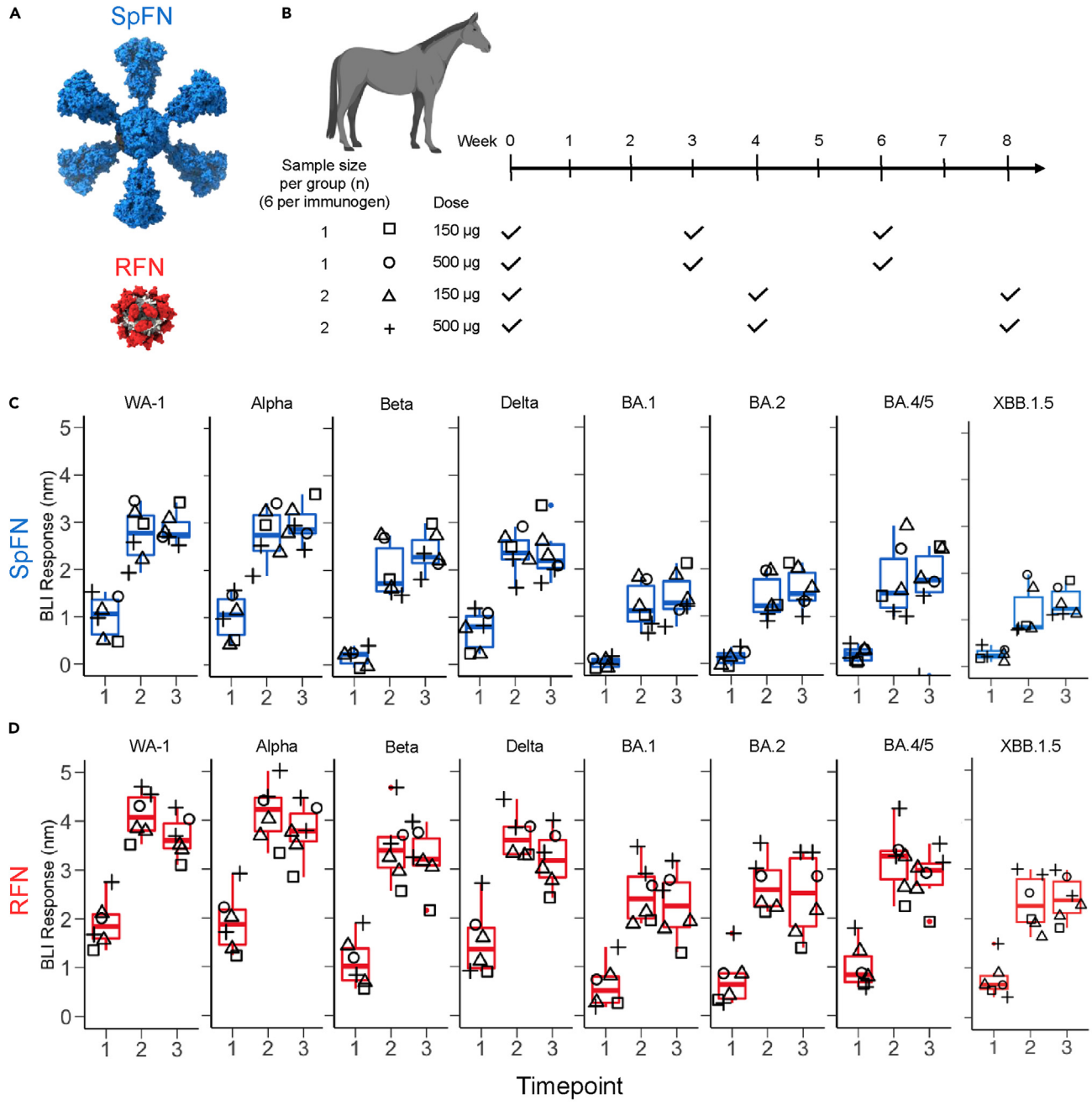

Figure 1. Robust RBD binding antibody responses elicited in the equine model

(A) Structural model of immunogens, Spike ferritin nanoparticle (SpFN) in blue and receptor binding domain ferritin nanoparticle (RFN) in red.

(B) Immunization schema for equine hyperimmune SARS-CoV-2-reactive sera generation (n = 12). Horses C9-C14 were immunized with SpFN, and horses C15-C20 were immunized with RFN, with CFA adjuvant for prime, and IFA for the subsequent two immunizations. Immunization schedules are depicted as square (150 µg dose at 0, 3, and 6 weeks), circle (500 µg dose at 0, 3, and 6 weeks), triangle (150 µg dose at 0, 4, and 8 weeks), and plus sign (500 µg dose at 0, 4, and 8 weeks).

(C and D) SARS-CoV-2 VoC RBD binding levels measured by BLI. (C) SpFN immunized group (blue), (D) RFN immunized group (red). Symbols are matched to the immunization schema shown in (B).

dose (Figure S2).The major difference between the SpFN and RFN immunization groups was the magnitude of RBD binding responses, with RFN typically eliciting 0.5–1 nm higher responses compared to SpFN, as measured by BLI (Figures 1C and 1D; Tables S3–S5) and 0.7–2.6 times higher titer as measured by ELISA (Table S2).

Spike ferritin nanoparticle - and receptor binding domain ferritin nanoparticle -elicited equine serum neutralizes severe acute respiratory syndrome coronavirus-2 variants of concern and severe acute respiratory syndrome coronavirus-1 in a pseudovirus assay

Neutralizing antibody responses were assessed against SARS-CoV-2 WA-1, a select set of SARS-CoV-2 VoC, and SARS-CoV-1 after each immunization (Figure 2A and Tables S6–S8). Following the first immunization, both SpFN and RFN immunized groups showed strong neutralizing ID_{50} titers against WA-1, Alpha, and Delta VoC, with intermediate levels against the Beta VoC. Five SpFN-immunized animals and two RFN-immunized animals had detectable ID_{50} neutralization titers (>50) against Omicron variants. Only one animal from each group showed low ID_{50} neutralization titers against the BA.5 VoC, and only one SpFN-immunized animal showed neutralization titer against Omicron XBB.1.5. SpFN-immunized animals had higher ID_{50} values against all pseudoviruses tested, compared to the RFN-immunized animals (Table S6). WA-1 ID_{50} geometric mean titers (GMT) measured after the first immunization were 3,141 for SpFN-immunized animals and 1,633 for RFN-immunized animals (Figures 2A and Table S6).

After the second immunization, all animals showed increased neutralization potency against the SARS-CoV-2 VoC, with all animals now showing neutralization against Omicrons including XBB.1.5, and SARS-CoV-1, and all except one showing neutralization against BA.5 (Figures 2A and Table S7). In general, the RFN-immunized group titers surpassed those of the SpFN group at this timepoint, though the difference was insignificant; they also showed greater variance than the SpFN group across all SARS-CoV-2 pseudovirions tested (Figures 2A and Tables S6–S8). Of note, for most pseudoviruses except Beta and Omicrons BA.1 and XBB.1.5, the ID_{50} titers from RFN-immunized animals decreased between the second and third timepoint, while SpFN-elicited titers slightly increased or remained constant between the same timepoints (Figure 2A).

Most SARS-CoV-2 VoC ID_{50} GMT were at a level between those of SARS-CoV-2 WA-1 (high) and SARS-CoV-1 (low), except for recent Omicron strains BA.5 and XBB.1.5, which were both consistently more difficult to neutralize compared to SARS-CoV-1 (Figures 2A and Tables S6–S8). SpFN-elicited neutralization was 3- and 5-fold lower for Beta and Omicron BA.1 variants compared with WA-1, with RFN-elicited neutralization titers 8- and 13-fold lower for the same variants relative to WA-1. The Omicron BA.5 neutralization elicited by SpFN was 40-fold lower, and RFN ID_{50} titers were 70-fold lower, compared to WA-1. The Omicron XBB.1.5 neutralization elicited by SpFN was 27-fold lower, and RFN ID_{50} titers were 13-fold lower, compared to WA-1.

For both nanoparticle immunogens SpFN and RFN, there was clear induction of potent cross-reactive neutralizing antibodies against SARS-CoV-2 WA-1, VoCs, and SARS-CoV-1. We noted a strong positive correlation between the homologous WA-1 neutralization titers and the SARS-CoV-1 titers, with approximately a 10-fold lower level for SARS-CoV-1 neutralization (Figure 2B). Furthermore, analysis of the BLI-measured RBD-binding levels and neutralization ID_{50} titers for all VoCs showed clear correlations (Figure 2C). We observed for each VoC, there is a different starting setpoint following the initial immunization titer, and slope to the correlation, dictated by the binding and neutralization levels measured for the equine sera against each virus over the three-immunization schedule.

Spike ferritin nanoparticle- and receptor binding domain ferritin nanoparticle-elicited equine serum antibodies can bind genetically distant receptor binding domains

To further assess the breadth of antibody binding specificity, we utilized a diverse set of twelve sarbecovirus RBDs as representative of sarbecovirus clades 1 (1a and 1b), 2, 3, and 4 (Figure 3A; Figure S2). As viral or pseudovirus assays have not been developed for the majority of these divergent sarbecoviruses and given the reasonable correlation between RBD-binding and neutralization for SARS-CoV-2 VoCs, we utilized RBD-binding and the BLI platform as a measure of the immune breadth. After the first immunization, clade 1b average binding responses were 0.43 nm (SpFN) and 1.16 nm (RFN); clade 1a were 0.16 nm (SpFN) and 0.57 nm (RFN); clade 2 were 0.13 nm (SpFN) and 0.56 nm (RFN); clade 3 were 0.21 nm (SpFN) and 0.49 nm (RFN); and clade 4 were 0.21 nm (SpFN) and 0.43 nm (RFN). At the second timepoint, SpFN and RFN elicited significantly increased responses compared to the first timepoint (p-values <0.005); the SpFN group response increased between 4.2- and 7.2-fold while the RFN group increased between 2.6- and 4.0-fold. The observed RFN response averages were ~1.7-, ~1.9-, ~2.4-, ~2.2, and 1.9-fold higher than SpFN response averages for clades 1b, 1a, 2, 3, and 4, respectively. At the third timepoint, recorded responses for SpFN increased while RFN responses remained stable; peak activity was measured at the second timepoint for RFN-immunized animals, while peak activity was observed at the third timepoint for SpFN-immunized animals. We saw that the RFN-immunized group exhibited consistently higher RBD binding, compared to the SpFN group, at each timepoint, and showed a greater degree of cross-reactivity compared to the SpFN group (Figures 3B and S2).

To further evaluate the breadth of the antibody binding response, we evaluated binding to MERS-CoV RBD molecules from the England1 (Eng1) and EMC/2012 (EMC) strains. In general, responses were low except for a subset of animals at specific timepoints, where signal intensities approached 0.3 nm for either one or both MERS-CoV RBD molecules (Figures S3A and S3B). To further determine if the cross-reactive responses were IgG mediated, we purified equine IgG from serum to assess the specificity of binding (Figure S3C). We then verified that the binding response was specific and titratable to WA-1, SARS-CoV-1, and MERS-CoV using both BLI and ELISA (Figures S3D and S3E). To assess whether the binding IgG-mediated responses to MERS had additional inhibitory capacity, we measured the inhibitory effect of the IgG on DPP4 receptor binding. The IgG from animals C12, C15 and C19 were able to exert DPP4 blocking activity, but this activity reached only 25% inhibition at 10 mg/mL concentration (Figure S3F).

To contextualize antigenic recognition and sequence distance across sarbecoviruses and visualize the breadth elicited by RFN and SpFN immunization, we plotted the BLI binding responses (depicted as contours) using a phylogenetic tree of sarbecovirus RBDs, with each tested RBD as a distinct reference point. Amino acid sequence distance is reflected by distance on the tree, while contour height is represented

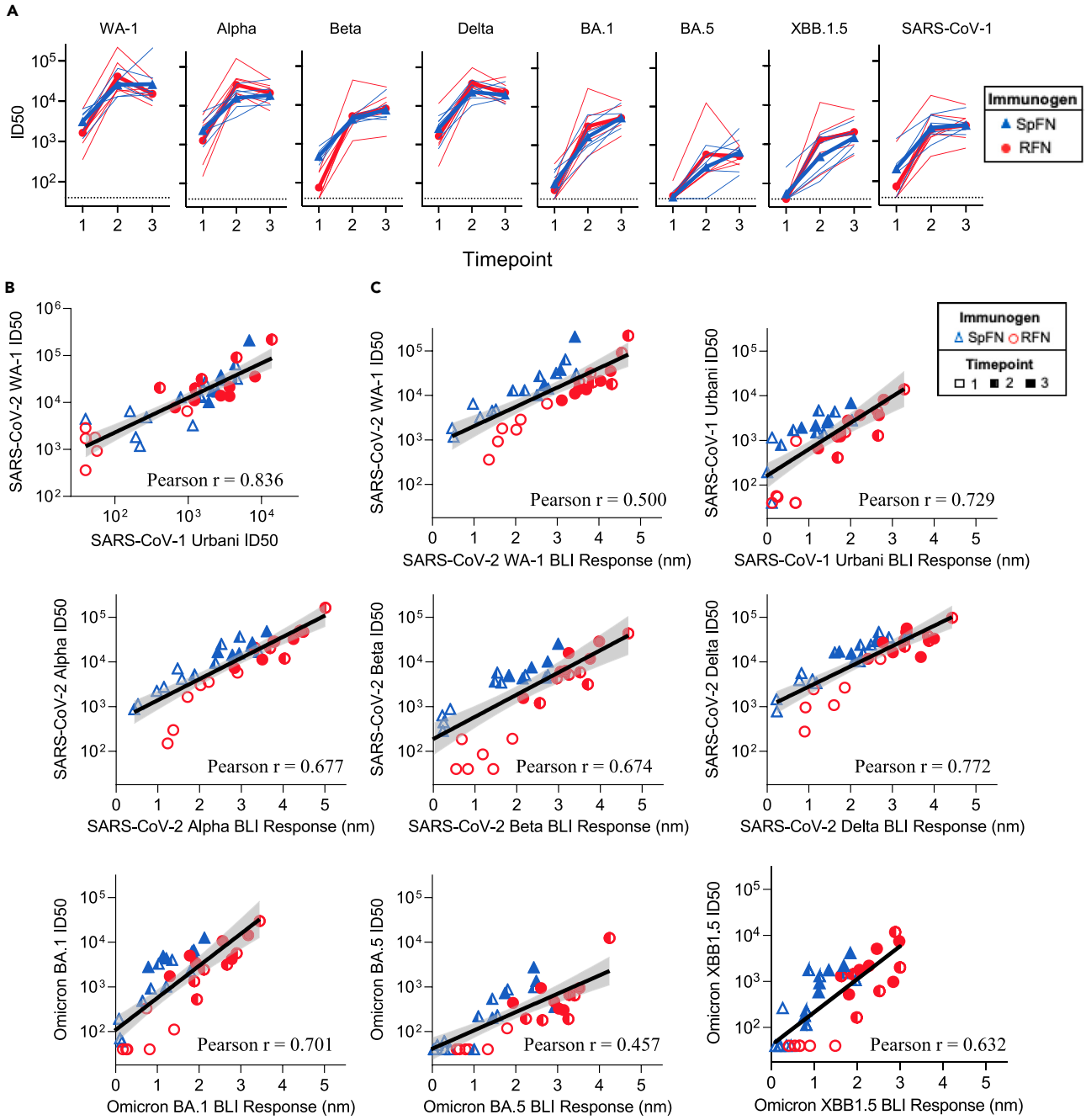

Figure 2. Sarbecovirus cross-reactive neutralization and binding capacity

(A) Pseudovirus neutralization (ID50 values) of WA-1, Alpha, Beta, Delta, Omicron BA.1, Omicron BA.5, Omicron XBB.1.5, and SARS-CoV-1. Thin lines represent individual animals, and the bold line depicts the geometric mean (blue, triangle: SpFN, red, circle: RFN).

(B) Correlation between SARS-CoV-2 WA-1 and SARS-CoV-1 Urbani pseudovirus neutralization titers (ID50), the black line depicts the locally weighted smoothing line and gray shading is the 95% confidence interval around the smoothing line.

(C) Correlation between BLI RBD-binding responses and pseudovirus neutralization titer (ID50), for each SARS-CoV-2 VoC and SARS-CoV-1. Pearson correlation coefficient calculation (r) assumed Gaussian distribution, and a two-tailed P value was calculated using GraphPad.

by BLI binding response (Figure 3C). The contour map interpolates binding measured at each point to better gauge the elicited breadth and potency.

In both SpFN- and RFN-immunized animals, the peak immune responses are detected at the antigen-matched homologous WA-1 strain for all three timepoints. Following each immunization, the SpFN-elicited breadth increased while the RFN-immune response after the second

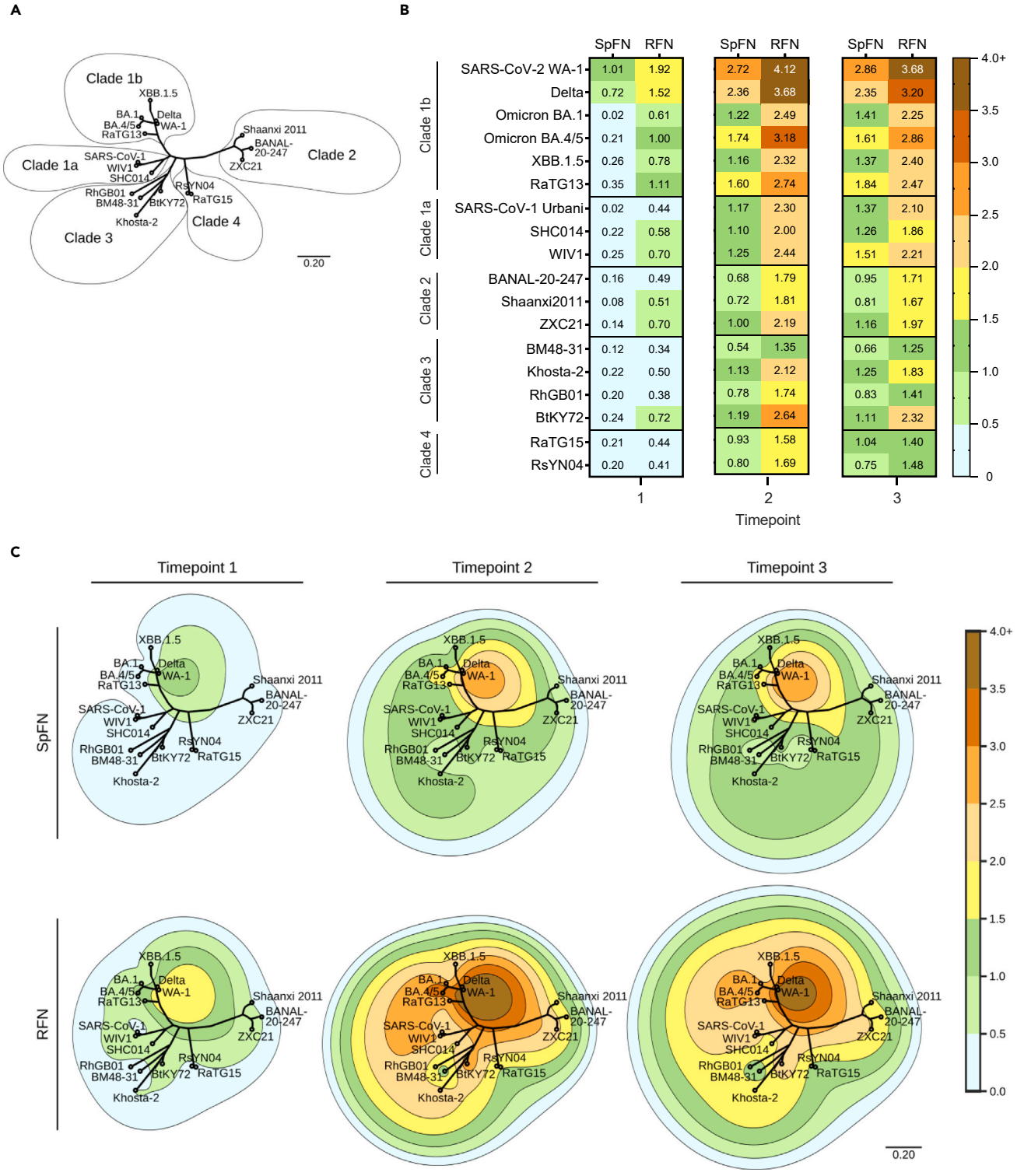

Figure 3. Cross-reactive RBD-binding response against genetically distant sarbecoviruses

(A) Phylogenetic tree, based on the RBD amino acid sequences of SARS-CoV-2 VoC and sarbecoviruses.

(B) Average serum binding responses (nm) to sarbecovirus RBD molecules measured by BLI for SpFN- and RFN-immunized animals (timepoints indicated at base of the plot).

Figure 3. *Continued*

(C) Contour-phylogenetic plots of binding of SpFN and RFN immunized animal sera to sarbecovirus RBD molecules. X and Y coordinates are determined by a phylogenetic tree of the RBD amino acid sequences, and contour height determined by detected BLI serum binding. Interpolation and extrapolation of binding data (elevation) between points on the phylogenetic tree was determined by a thin plate radial basis function (r2*log(r)) using the scipy python package. For clarity, extrapolated values higher than the maximum measured binding were truncated at the maximum binding for the timepoint.

and third immunization was similar. As seen for the SARS-CoV-2 binding responses, RFN-immunized animal sera showed a higher binding signal to the panel of sarbecovirus RBDs compared to SpFN-immunized animals. The SpFN-elicited immune response after a single immunization was quite focused at WA-1 and Delta with minimal breadth, with an increase in breadth following subsequent immunizations. In the case of RFN immunization, there was reasonable RBD-binding breadth after a single immunization, which increased and expanded after the second immunization.

The contour map is a useful visualization tool to understand binding levels in the context of sarbecovirus sequence differences, as binding levels do not directly change as a function of sequence distance. For instance, serum binding levels to BA.1 were comparable to the distantly related clade 3 BtKY72 and Khosta-2 and clade 2 ZXC21 sarbecovirus RBD molecules. Also, within a given clade, it is clear that differential binding levels were seen, e.g., RhGB01 and BM48-31 showed lower binding than Khosta-2 and BtKY72. The contour map also shows a rapid reduction in binding within the clade 1b sarbecoviruses, from the immunogen-matched WA-1 at the peak compared to the Omicron BA.1 and BA.4/5 variants, though less so for XBB.1.5.

Purified equine IgG protects against virus challenge in the K18-hACE2 mouse model

To assess the ability of the elicited equine antibodies to provide useful protective properties against SARS-CoV-2 infection, we carried out a proof-of-principle *in vivo* protection study using K18-hACE2 transgenic mice, with SARS-CoV-2 Omicron XBB.1.5 strain as the challenge strain (Figure 4A). Polyclonal IgG was purified from the pooled equine serum obtained following either the third SpFN or RFN immunization respectively. A control human IgG1 antibody, MZ4 that is active against Zika and Dengue[56] was used as a control. Groups of 10 K18-hACE2 mice were passively immunized by the intraperitoneal injection of 200 μL of SpFN- or RFN-derived purified poly IgG (concentration OD280 = 30, ~20 mg/mL, equivalent to 200 mg per kg body weight), or 400 μg of the MZ4 IgG1 isotype control (equivalent to 20 mg per kg body weight), followed 24 h later by intranasal challenge with 1.25×10^4 PFU of SARS-CoV-2 Omicron XBB.1.5. The mice were assessed at day 2 for virus titer in bronchoalveolar lavage (BAL) and monitored for 14 days for weight loss, survival, clinical score (Figure 4). Polyclonal IgG from both SpFN- and RFN-immunized horses provided significant disease protection in comparison to the control group. RFN-derived poly IgG significantly reduced the Omicron XBB.1.5 viral titers in BAL, with SpFN-derived poly IgG showing approximately 1-log lower geometric mean viral titers compared to the control group. In both the SpFN- and RFN-derived poly IgG treatment group, there was protection against weight loss, with significance from day 4–8.5 in the SpFN group, and from day 5–8 in the RFN group.

DISCUSSION

SARS-CoV-2 variants capable of immune escape continue to emerge and rapidly spread in the human population; thus, the continued development of innovative vaccines and therapeutics remains an ongoing effort. Small molecule inhibitors, convalescent plasma, mAbs, and mRNA and viral vector vaccines were effective at addressing the initial outbreak of the pandemic and provided protection and lessened infection severity. The emergence of highly mutated variants that evade many of these treatment and prevention modalities highlights the need for next-generation interventions. Bivalent mRNA vaccines, which encode the spike from WA-1 and Omicron BA.1 or BA.4/BA.5, elicit an immune response with improved protection.[57] However, Omicron BQ.1.1, and XBB.1 demonstrate increased immune evasion even with more recent vaccines, and evade clinically authorized therapeutics, such as bebtelovimab and sotrovimab.[21,58–61] Sotrovimab targets an epitope conserved between SARS-CoV-1 and SARS-CoV-2 WA-1,[61] indicating that new SARS-CoV-2 variants have specific mutations making them more immune evasive than more distantly related sarbecoviruses. As mAb-based therapies have been rendered ineffective with the emergence of new variants,[21,22,60,62,63] solutions utilizing antibody engineering, or mAb cocktails, have gained renewed focus.[53,60,64] In populations for whom vaccine efficacy is diminished, such as the immunocompromised, and for whom the use of currently available small molecule drugs is contraindicated, therapeutic lines of defense are urgently needed. Polyclonal IgG therapies currently appear more robust than mAb therapeutics – sera from vaccinated or convalescent human subjects retain activity, albeit diminished, against new variants.[21,22,60,62]

The nanoparticle vaccines used in our study, based on WA-1 spike (SpFN) and RBD (RFN), were previously demonstrated to elicit potent and cross-reactive neutralizing antibodies, ACE2 inhibition, IgG opsonization, and protection against viral challenge after 1–3 immunizations.[49–55,65,66] Most recently SpFN adjuvanted with ALFQ was assessed for immunogenicity in a phase I study in antigen-naïve humans. After three immunizations, a significant breadth of immune response was observed including neutralizing responses against multiple diverse sarbecoviruses including SARS-CoV-1 Urbani and the SARS-CoV-2 Omicron XBB.1.5 VoC. Horses have long been a rapidly developable source of high potency, hyperimmune antibodies.[36] Through the immunization of horses with next-generation nanoparticle vaccines, using a short time course, we show that in all animals, vaccination by SpFN or RFN elicited robust and high titer SARS-CoV-2 VoC and SARS-CoV-1 binding and pseudovirus neutralization titers within 1–2 immunizations. The RBD-targeted responses and neutralization potency generated in the equine model were strong, and at levels that match those shown to be protective in previous animal challenge studies.[50,51,65] Analysis of the binding response against a panel of sarbecovirus showed a broad response against all sarbecovirus

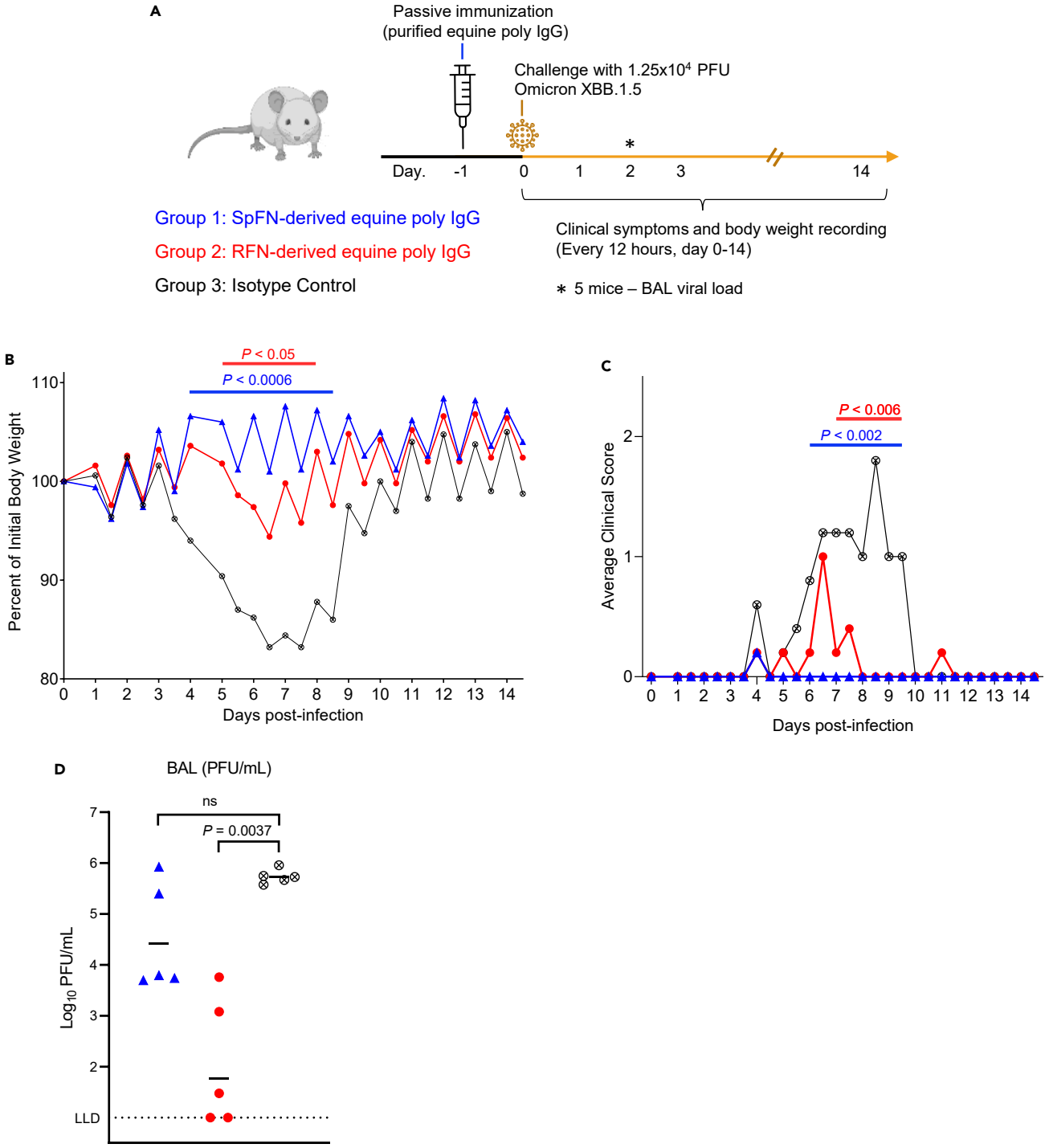

Figure 4. Passive immunization with purified equine IgG protect mice from SARS-CoV-2 XBB.1.5 challenge

(A) Schematic of K18-hACE2 mice SARS-CoV-2 challenge study. Mice (n = 10/group, 5 female, 5 male) received an intraperitoneal injection of purified IgG from SpFN-immunized horses (blue), or RFN-immunized horses (red), or human IgG1 isotype control mAb (black), one day prior to challenge with 1.25 × 10^4 PFU of SARS-CoV-2 virus (Omicron XBB.1.5).

(B) Body weight measurements for K18-hACE2 mice over the course of the challenge study (n = 5/group). Percentage of initial weight is plotted. Isotype control mAb (black open X circle), or SpFN-purified IgG (blue triangle) or RFN-purified IgG (red circle). Significant difference for each measurement timepoint between each group compared to the antibody isotype control group, as assessed by t-test is indicated by a horizontal line.

Figure 4. *Continued*

(C) Average cinical score measurements of the K18-hACE2 study groups (n = 5/group). Isotype control mAb (black open X circle), or SpFN-purified IgG (blue triangle) or RFN-purified IgG (red circle). Significant difference for each measurement timepoint between each group compared to the antibody isotype control group, as assessed by t-test is indicated by a horizontal line above the plot.

(D) SARS-CoV-2 viral loads in BAL, were measured 2 days post-challenge in a subset of animals (n = 5/group) by plaque assay. BAL (PFU/mL) viral levels in the two study groups were compared for significance against the control group using a Kruskal-Wallis ANOVA test followed by post hoc Dunn's multiple comparison test.

clades. Analysis of the pseudovirus neutralization titers and BLI shows a correlation between RBD binding and ID_{50} neutralization titers. This correlation suggests that the rapid BLI-based assay can be leveraged in the absence of pseudovirus assays, or as a preliminary assay to gauge immunogenicity of convalescent sera. We also observed MERS RBD-binding and DPP4-blocking capacity from the equine sera, which highlights the capacity for the development of broad anti-coronaviral responses in the equine model. Detailed molecular analysis of the composition of the polyclonal response is absent from our study. In general, there have been limited studies analyzing equine monoclonal antibodies to provide further understanding or explanation for the broad equine immune responses that are elicited against specific immunogens. The diversity can be somewhat explained by the extensive utilization of antibody junctional diversity. While V and J chain diversity may be limited, D-gene usage and combination can range from 0 to 111 nucleotides providing extensive structural and molecular diversity.[67]

Antigenic cartography plots were initially developed for the influenza virus and have more recently been utilized to map SARS-CoV-2 immune responses. The maps display patterns in antigenicity, allowing for an improved understanding of the breadth elicited by different vaccination and natural infection histories.[68,69] However, the antigenic cartography maps have altered coordinates as the immune response alters, and do not inherently display information related to neutralization titer level or antigen sequence diversity, which limits their interpretability and applicability. Using equine sera with a broad immune response, we coupled the BLI RBD-binding signals to a phylogenetic tree, to generate a contour map to visualize binding response levels in the context of sarbecovirus sequence diversity. The contour map highlights the broad and robust sarbecovirus response seen with both SpFN and RFN immunization. The binding data can be substituted with neutralization titer data, or other immune measurements, to allow combined visualization of responses versus sequence diversity. These plots can provide insights to aid SARS-CoV-2 vaccine selection or pan-sarbecovirus or pan-coronavirus vaccine component selection.

To evaluate the elicited equine serum, we carried out a proof-of-principle SARS-CoV-2 challenge and protection study using Omicron XBB.1.5 as the challenge strain. We purified the polyclonal IgG portion from the equine sera and dosed K18-hACE2 mice at levels (0.2 g/kg) similar to a typical human intravenous IgG administration,[67] and compared to a human IgG1 control antibody.[68] In both SpFN- and RFN-derived purified polyclonal IgG, there was significant protection from disease clinical symptoms and animal weight loss. At day 2, lung BAL was lower in both treatment groups, but significantly lower in the RFN-polyclonal IgG treatment group. The Omicron XBB.1.5 is typically not a lethal virus, but 1 animal in the control group did die. The observed protective capability is quite striking as the horses were immunized with SpFN and RFN immunogens based on the ancestral WA-1 sequence. The binding and neutralizing responses against XBB.1.5 in the equine sera (Figures 1 and 2) were encouraging but the levels of protection against disease and viral titers seen following the challenge are encouraging for further development efforts, given that more potent Omicron-specific polyclonal response can be rapidly generated using updated SpFN or RFN immunogens.

The use of equine polyclonal IgG in humans can result in adverse immune reactions that range from mild to severe adverse events, such as anaphylaxis or serum sickness. Refinements in the production of equine sera products have lessened these responses, such as improved product sterility, F(ab')2 preparation, and further purification steps to ensure product consistency and removal of non-immune sera components. Clinical studies using equine polyclonal F(ab')2 to treat SARS-CoV-2 showed some protective and beneficial effects, while adverse events of special interest were mild or moderate and no anaphylaxis was reported.[70,71]

In summary, SpFN and RFN immunization of horses elicited potently neutralizing and protective sera within six weeks. In comparison, horses immunized with MERS-CoV virus-like particles required five immunizations and a higher dose of immunogen to achieve equivalent levels.[40] Similar to the responses seen in prior pre-clinical immunization studies,[49–51,53] the equine sera derived from SpFN or RFN immunization displayed broad sarbecovirus activity. In the context of pan-coronavirus vaccine development, polyclonal therapeutic development, and the effort to elicit broadly protective immune responses, the observations from this study are encouraging. As a proof-of-concept, by combining ferritin nanoparticle vaccines alongside the equine model, we demonstrate that it is possible to rapidly generate broadly reactive high titer sera in an emerging infectious disease scenario.

Limitations of the study

The SpFN and RFN immunogens used in this study were based on the SARS-CoV-2 WA-1 strain and elicited broad sarbecovirus binding and neutralization levels. Immunization of horses with SpFN or RFN immunogen versions based on Omicron strains, or a cocktail of similar nanoparticle immunogens including other coronaviruses would have allowed the characterization and assessment of expanded breadth or titers of binding and neutralization. Binding and neutralization titers from the equine sera assessed in this study have variable correlations depending on the SARS-CoV-2 viral variant. Further assessment of BLI binding and neutralization titers using alternate species sera species or from animals immunized with heterologous or extended immunization regimens would aid the understanding of the binding-neutralization correlation. In this study, we did not characterize the equine F(ab')2 component, which is most directly applicable to human treatment regimens. This

study characterized protection against SARS-CoV-2 Omicron XBB.1.5 strain, but the characterization of the protective response against other SARS-CoV-2 strains in the K18-ACE2 model, or in Syrian golden hamsters, or non-human primates would further aid in the development of our understanding of the protective efficacy of equine sera against SARS-CoV-2 disease. Molecular, structural, and immunogenetic characterization of the equine polyclonal immune response was not carried out, and this would enable further understanding of the antibody response. Ultimately, the assessment of the ability of hyperimmune equine sera to provide protection or treatment of SARS-CoV-2 in humans is the most meaningful barometer.

RESOURCE AVAILABILITY

Lead contact

Further information and requests for resources and reagents should be directed to and will be fulfilled by the Lead Contact, M. Gordon Joyce (gjoyce@eidresearch.org).

Materials availability

All reagents will be made available on request after completion of a Materials Transfer Agreement.

Data and code availability

- All data supporting the findings of this study are found within the article and its Supplementary Information.
- This article does not report the original code.
- Any additional information required to reanalyze the data reported in this article is available from the lead contact author upon request.

ACKNOWLEDGMENTS

We thank M. Amare, M. Taddesse, E.Sondergaard, T. Mbehratu, J. Headley, J. Lay and S. Daye for programmatic, administrative, and regulatory support and planning. Research was carried out under a Cooperative Research and Development Agreement between BSV, WRAIR, and HJF. Part of the work was funded by the U.S. Defense Health Agency, the U.S. Department of the Army, and a cooperative agreement between The Henry M. Jackson Foundation for the Advancement of Military Medicine, Inc. and the U.S. Department of Defense (W81XWH-18-2-0040). Material has been reviewed by the Walter Reed Army Institute of Research. There is no objection to its presentation and/or publication. The opinions or assertions contained herein are the private views of the authors, and are not to be construed as official, or as reflecting true views of the Department of the Army or the Department of Defense or Henry M. Jackson Foundation for the Advancement of Military Medicine, Inc.

AUTHOR CONTRIBUTIONS

Conceptualization, J.Kau., K.M., M.G.J.; Investigation, E.J.M., W.C.C., W-H.C., A.H., P.V.T., J.L.J., M.C., R.S.S., C.E.P., P.A.R., S.S., C.K., J.K., C.C., T.C., J.H., L.K., T.H., K.L., J.G., M.R., D.D., W.W.R., S.V.M., A.F., K.Mur., G.D.G., K.M., J.K., M.G.J. Data Curation, E.J.M., W.C.C., W-H.C., A.H., P.V.T., J.L.J., W.W.R., M.G.J., Writing – Original Draft, E.J.M., W.C.C., M.G.J.; Writing – Review & Editing, All authors; Visualization, E.J.M., W.C.C., W-H.C., A.H., P.V.T., M.G.J.; Supervision, N.D.C., S.V., G.D.G., S.J.K., W.W.R. N.L.M., K.M., and M.G.J. Funding Acquisition, J.Kau., N.L.M., K.M., and S.V.

DECLARATION OF INTERESTS

W.H.C, A.H., P.V.T., J.L.J., K.M. and M.G.J. are named inventors on provisional patents describing SpFN molecules. S.J.K., V.D., N.L.M., and K.M. are named inventors on provisional patents describing monoclonal antibodies against coronaviruses. M.G.J. is named as an inventor on international patent application WO/2018/081318 and U.S. patents 10,960,070, and 11,964,010 entitled "Prefusion coronavirus spike proteins and their use." K.M. is a current employee of Pfizer and may, therefore, be a shareholder. A.F., K.Mur., and J.Kau. are former or current employees of B.S.V. The other authors declare no competing interests.

STAR★METHODS

Detailed methods are provided in the online version of this paper and include the following:

SUPPLEMENTAL INFORMATION

Supplemental information can be found online at https://doi.org/10.1016/j.isci.2024.110624.

Received: January 8, 2024
Revised: May 23, 2024
Accepted: July 29, 2024
Published: August 23, 2024

REFERENCES

1. Starr, T.N., Zepeda, S.K., Walls, A.C., Greaney, A.J., Alkhovsky, S., Veesler, D., and Bloom, J.D. (2022). ACE2 binding is an ancestral and evolvable trait of sarbecoviruses. Nature *603*, 913–918. https://doi.org/10.1038/s41586-022-04464-z.
2. Wells, H.L., Letko, M., Lasso, G., Ssebide, B., Nziza, J., Byarugaba, D.K., Navarrete-Macias, I., Liang, E., Cranfield, M., Han, B.A., et al. (2021). The evolutionary history of ACE2 usage within the coronavirus subgenus Sarbecovirus. Virus Evol. *7*, veab007. https://doi.org/10.1093/ve/veab007.
3. Boni, M.F., Lemey, P., Jiang, X., Lam, T.T.Y., Perry, B.W., Castoe, T.A., Rambaut, A., and Robertson, D.L. (2020). Evolutionary origins of the SARS-CoV-2 sarbecovirus lineage responsible for the COVID-19 pandemic. Nat. Microbiol. *5*, 1408–1417. https://doi.org/10.1038/s41564-020-0771-4.
4. Heffron, A.S., McIlwain, S.J., Amjadi, M.F., Baker, D.A., Khullar, S., Armbrust, T., Halfmann, P.J., Kawaoka, Y., Sethi, A.K., Palmenberg, A.C., et al. (2021). The landscape of antibody binding in SARS-CoV-2 infection. PLoS Biol. *19*, e3001265. https://doi.org/10.1371/journal.pbio.3001265.
5. Racine, T., Denizot, M., Pannetier, D., Nguyen, L., Pasquier, A., Raoul, H., Saluzzo, J.F., Kobinger, G., Veas, F., and Herbreteau, C.H. (2019). In Vitro Characterization and In Vivo Effectiveness of Ebola Virus Specific Equine Polyclonal F(ab')2. J. Infect. Dis. *220*, 41–45. https://doi.org/10.1093/infdis/jiz068.
6. Andreano, E., Piccini, G., Licastro, D., Casalino, L., Johnson, N.V., Paciello, I., Dal Monego, S., Pantano, E., Manganaro, N., Manenti, A., et al. (2021). SARS-CoV-2 escape from a highly neutralizing COVID-19 convalescent plasma. Proc. Natl. Acad. Sci. USA *118*, e2103154118. https://doi.org/10.1073/pnas.2103154118.
7. Chen, R.E., Zhang, X., Case, J.B., Winkler, E.S., Liu, Y., VanBlargan, L.A., Liu, J., Errico, J.M., Xie, X., Suryadevara, N., et al. (2021). Resistance of SARS-CoV-2 variants to neutralization by monoclonal and serum-derived polyclonal antibodies. Nat. Med. *27*, 717–726. https://doi.org/10.1038/s41591-021-01294-w.
8. Collier, D.A., De Marco, A., Ferreira, I.A.T.M., Meng, B., Datir, R.P., Walls, A.C., Kemp, S.A., Bassi, J., Pinto, D., Silacci-Fregni, C., et al. (2021). Sensitivity of SARS-CoV-2 B.1.1.7 to mRNA vaccine-elicited antibodies. Nature *593*, 136–141. https://doi.org/10.1038/s41586-021-03412-7.
9. Dussupt, V., Sankhala, R.S., Mendez-Rivera, L., Townsley, S.M., Schmidt, F., Wieczorek, L., Lal, K.G., Donofrio, G.C., Tran, U., Jackson, N.D., et al. (2021). Low-dose in vivo protection and neutralization across SARS-CoV-2 variants by monoclonal antibody combinations. Nat. Immunol. *22*, 1503–1514. https://doi.org/10.1038/s41590-021-01068-z.
10. Laurini, E., Marson, D., Aulic, S., Fermeglia, A., and Pricl, S. (2021). Molecular rationale for SARS-CoV-2 spike circulating mutations able to escape bamlanivimab and etesevimab monoclonal antibodies. Sci. Rep. *11*, 20274. https://doi.org/10.1038/s41598-021-99827-3.
11. Wang, Q., Guo, Y., Iketani, S., Nair, M.S., Li, Z., Mohri, H., Wang, M., Yu, J., Bowen, A.D., Chang, J.Y., et al. (2022). Antibody evasion by SARS-CoV-2 Omicron subvariants BA.2.12.1, BA.4, & BA.5. Nature *608*, 603–608. https://doi.org/10.1038/s41586-022-05053-w.
12. Wang, R., Zhang, Q., Zhang, R., Aw, Z.Q., Chen, P., Wong, Y.H., Hong, J., Ju, B., Shi, X., Ding, Q., et al. (2022). SARS-CoV-2 Omicron Variants Reduce Antibody Neutralization and Acquire Usage of Mouse ACE2. Front. Immunol. *13*, 854952. https://doi.org/10.3389/fimmu.2022.854952.
13. Tuekprakhon, A., Nutalai, R., Dijokaite-Guraliuc, A., Zhou, D., Ginn, H.M., Selvaraj, M., Liu, C., Mentzer, A.J., Supasa, P., Duyvesteyn, H.M.E., et al. (2022). Antibody escape of SARS-CoV-2 Omicron BA.4 and BA.5 from vaccine and BA.1 serum. Cell *185*, 2422–2433.e13. https://doi.org/10.1016/j.cell.2022.06.005.
14. Cao, Y., Yisimayi, A., Jian, F., Song, W., Xiao, T., Wang, L., Du, S., Wang, J., Li, Q., Chen, X., et al. (2022). BA.2.12.1, BA.4 and BA.5 escape antibodies elicited by Omicron infection. Nature *608*, 593–602. https://doi.org/10.1038/s41586-022-04980-y.
15. Iketani, S., Liu, L., Guo, Y., Liu, L., Chan, J.F.W., Huang, Y., Wang, M., Luo, Y., Yu, J., Chu, H., et al. (2022). Antibody evasion properties of SARS-CoV-2 Omicron sublineages. Nature *604*, 553–556. https://doi.org/10.1038/s41586-022-04594-4.
16. Liu, L., Iketani, S., Guo, Y., Chan, J.F.W., Wang, M., Liu, L., Luo, Y., Chu, H., Huang, Y., Nair, M.S., et al. (2022). Striking antibody evasion manifested by the Omicron variant of SARS-CoV-2. Nature *602*, 676–681. https://doi.org/10.1038/s41586-021-04388-0.
17. Mannar, D., Saville, J.W., Zhu, X., Srivastava, S.S., Berezuk, A.M., Tuttle, K.S., Marquez, A.C., Sekirov, I., and Subramaniam, S. (2022). SARS-CoV-2 Omicron variant: Antibody evasion and cryo-EM structure of spike protein-ACE2 complex. Science *375*, 760–764. https://doi.org/10.1126/science.abn7760.
18. McCallum, M., Czudnochowski, N., Rosen, L.E., Zepeda, S.K., Bowen, J.E., Walls, A.C., Hauser, K., Joshi, A., Stewart, C., Dillen, J.R., et al. (2022). Structural basis of SARS-CoV-2 Omicron immune evasion and receptor engagement. Science *375*, 864–868. https://doi.org/10.1126/science.abn8652.
19. Nabel, K.G., Clark, S.A., Shankar, S., Pan, J., Clark, L.E., Yang, P., Coscia, A., McKay, L.G.A., Varnum, H.H., Brusic, V., et al. (2022). Structural basis for continued antibody evasion by the SARS-CoV-2 receptor binding domain. Science *375*, eabl6251. https://doi.org/10.1126/science.abl6251.
20. Wang, P., Nair, M.S., Liu, L., Iketani, S., Luo, Y., Guo, Y., Wang, M., Yu, J., Zhang, B., Kwong, P.D., et al. (2021). Antibody resistance of SARS-CoV-2 variants B.1.351 and B.1.1.7. Nature *593*, 130–135. https://doi.org/10.1038/s41586-021-03398-2.
21. Planas, D., Bruel, T., Staropoli, I., Guivel-Benhassine, F., Porrot, F., Maes, P., Grzelak, L., Prot, M., Mougari, S., Planchais, C., et al. (2023). Resistance of Omicron subvariants BA.2.75.2, BA.4.6, and BQ.1.1 to neutralizing antibodies. Nat. Commun. *14*, 824. https://doi.org/10.1038/s41467-023-36561-6.
22. Lusvarghi, S., Pollett, S.D., Neerukonda, S.N., Wang, W., Wang, R., Vassell, R., Epsi, N.J., Fries, A.C., Agan, B.K., Lindholm, D.A., et al. (2022). SARS-CoV-2 BA.1 variant is neutralized by vaccine booster-elicited serum but evades most convalescent serum and therapeutic antibodies. Sci. Transl. Med. *14*, eabn8543. https://doi.org/10.1126/scitranslmed.abn8543.
23. Kurhade, C., Zou, J., Xia, H., Liu, M., Yang, Q., Cutler, M., Cooper, D., Muik, A., Sahin, U., Jansen, K.U., et al. (2022). Neutralization of Omicron sublineages and Deltacron SARS-CoV-2 by 3 doses of BNT162b2 vaccine or BA.1 infection. Emerg. Microb. Infect. *11*, 1828–1832. https://doi.org/10.1080/22221751.2022.2099305.
24. Bekliz, M., Adea, K., Vetter, P., Eberhardt, C.S., Hosszu-Fellous, K., Vu, D.L., Puhach, O., Essaidi-Laziosi, M., Waldvogel-Abramowski, S., Stephan, C., et al. (2022). Neutralization capacity of antibodies elicited through homologous or heterologous infection or vaccination against SARS-CoV-2 VOCs. Nat. Commun. *13*, 3840. https://doi.org/10.1038/s41467-022-31556-1.
25. Self, W.H., Wheeler, A.P., Stewart, T.G., Schrager, H., Mallada, J., Thomas, C.B., Cataldo, V.D., O'Neal, H.R., Jr., Shapiro, N.I., Higgins, C., et al. (2022). Neutralizing COVID-19 Convalescent Plasma in Adults Hospitalized With COVID-19: A Blinded, Randomized, Placebo-Controlled Trial. Chest *162*, 982–994. https://doi.org/10.1016/j.chest.2022.06.029.
26. Casadevall, A., Joyner, M.J., Pirofski, L.A., Senefeld, J.W., Shoham, S., Sullivan, D., Paneth, N., and Focosi, D. (2023). Convalescent plasma therapy in COVID-19: Unravelling the data using the principles of antibody therapy. Expet Rev. Respir. Med. *17*, 381–395. https://doi.org/10.1080/17476348.2023.2208349.
27. Joyner, M.J., Paneth, N., and Casadevall, A. (2023). Use of convalescent plasma in the treatment of COVID-19. Nat. Rev. Nephrol. *19*, 271. https://doi.org/10.1038/s41581-023-00690-4.
28. Franchini, M., Casadevall, A., Joyner, M.J., and Focosi, D. (2023). WHO Is Recommending against the Use of COVID-19 Convalescent Plasma in Immunocompromised Patients? Life *13*, 134. https://doi.org/10.3390/life13010134.
29. Senefeld, J.W., Paneth, N.S., Carter, R.E., Wright, R.S., Fairweather, D., Bruno, K.A., and Joyner, M.J. (2022). Late Treatment for COVID-19 With Convalescent Plasma. Chest *162*, e283–e284. https://doi.org/10.1016/j.chest.2022.07.029.

30. Gutiérrez, J.M., Lomonte, B., Sanz, L., Calvete, J.J., and Pla, D. (2014). Immunological profile of antivenoms: preclinical analysis of the efficacy of a polyspecific antivenom through antivenomics and neutralization assays. J. Proteonomics *105*, 340–350. https://doi.org/10.1016/j.jprot.2014.02.021.
31. Moreira-Soto, A., Arguedas, M., Brenes, H., Buján, W., Corrales-Aguilar, E., Díaz, C., Echeverri, A., Flores-Díaz, M., Gómez, A., Hernández, A., et al. (2021). High Efficacy of Therapeutic Equine Hyperimmune Antibodies Against SARS-CoV-2 Variants of Concern. Front. Med. *8*, 735853. https://doi.org/10.3389/fmed.2021.735853.
32. Ponchner, D. (2020). Antibodies for Trials as an Inexpensive COVID-19 Therapy (Scientific American).
33. da Costa, C.B.P., Martins, F.J., da Cunha, L.E.R., Ratcliffe, N.A., Cisne de Paula, R., and Castro, H.C. (2021). COVID-19 and Hyperimmune sera: A feasible plan B to fight against coronavirus. Int. Immunopharm. *90*, 107220. https://doi.org/10.1016/j.intimp.2020.107220.
34. Ledsgaard, L., Jenkins, T.P., Davidsen, K., Krause, K.E., Martos-Esteban, A., Engmark, M., Rørdam Andersen, M., Lund, O., and Laustsen, A.H. (2018). Antibody Cross-Reactivity in Antivenom Research. Toxins *10*, 393. https://doi.org/10.3390/toxins10100393.
35. Dixit, R., Herz, J., Dalton, R., and Booy, R. (2016). Benefits of using heterologous polyclonal antibodies and potential applications to new and undertreated infectious pathogens. Vaccine *34*, 1152–1161. https://doi.org/10.1016/j.vaccine.2016.01.016.
36. Pan, X., Wu, Y., Wang, W., Zhang, L., and Xiao, G. (2020). Development of horse neutralizing immunoglobulin and immunoglobulin fragments against Junin virus. Antivir. Res. *174*, 104666. https://doi.org/10.1016/j.antiviral.2019.104666.
37. Bermúdez-Méndez, E., Fuglsang-Madsen, A., Føns, S., Lomonte, B., Gutiérrez, J.M., and Laustsen, A.H. (2018). Innovative Immunization Strategies for Antivenom Development. Toxins *10*, 452.
38. Waghmare, A., Deopurkar, R.L., Salvi, N., Khadilkar, M., Kalolikar, M., and Gade, S.K. (2009). Comparison of Montanide adjuvants, IMS 3012 (Nanoparticle), ISA 206 and ISA 35 (Emulsion based) along with incomplete Freund's adjuvant for hyperimmunization of equines used for production of polyvalent snake antivenom. Vaccine *27*, 1067–1072. https://doi.org/10.1016/j.vaccine.2008.11.103.
39. Zheng, X., Wong, G., Zhao, Y., Wang, H., He, S., Bi, Y., Chen, W., Jin, H., Gai, W., Chu, D., et al. (2016). Treatment with hyperimmune equine immunoglobulin or immunoglobulin fragments completely protects rodents from Ebola virus infection. Sci. Rep. *6*, 24179. https://doi.org/10.1038/srep24179.
40. Zhao, Y., Wang, C., Qiu, B., Li, C., Wang, H., Jin, H., Gai, W., Zheng, X., Wang, T., Sun, W., et al. (2017). Passive immunotherapy for Middle East Respiratory Syndrome coronavirus infection with equine immunoglobulin or immunoglobulin fragments in a mouse model. Antivir. Res. *137*, 125–130. https://doi.org/10.1016/j.antiviral.2016.11.016.
41. Farizano Salazar, D.H., Achinelli, F., Colonna, M., Pérez, L., Giménez, A.A., Ojeda, M.A., Miranda Puente, S.N., Sánchez Negrette, L., Cañete, F., Martelotte Ibarra, O.I., et al. (2022). Safety and effectiveness of RBD-specific polyclonal equine F(ab)2 fragments for the treatment of hospitalized patients with severe Covid-19 disease: A retrospective cohort study. PLoS One *17*, e0274796. https://doi.org/10.1371/journal.pone.0274796.
42. Li, E., Han, Q., Bi, J., Wei, S., Wang, S., Zhang, Y., Liu, J., Feng, N., Wang, T., Wu, J., et al. (2023). Therapeutic equine hyperimmune antibodies with high and broad-spectrum neutralizing activity protect rodents against SARS-CoV-2 infection. Front. Immunol. *14*, 1066730. https://doi.org/10.3389/fimmu.2023.1066730.
43. Rodriguez-Nuñez, M., Cepeda, M.D.V., Bello, C., Lopez, M.A., Sulbaran, Y., Loureiro, C.L., Liprandi, F., Jaspe, R.C., Pujol, F.H., and Rangel, H.R. (2023). Neutralization of Different Variants of SARS-CoV-2 by a F(ab')2 Preparation from Sera of Horses Immunized with the Viral Receptor Binding Domain. Antibodies *12*, 80. https://doi.org/10.3390/antib12040080.
44. Liu, Z., Wu, H., Egland, K.A., Gilliland, T.C., Dunn, M.D., Luke, T.C., Sullivan, E.J., Klimstra, W.B., Bausch, C.L., and Whelan, S.P.J. (2022). Human immunoglobulin from transchromosomic bovines hyperimmunized with SARS-CoV-2 spike antigen efficiently neutralizes viral variants. Hum. Vaccines Immunother. *18*, 1940652. https://doi.org/10.1080/21645515.2021.1940652.
45. Tang, J., Grubbs, G., Lee, Y., Wu, H., Luke, T.C., Egland, K.A., Bausch, C.L., Sullivan, E.J., and Khurana, S. (2022). Increased Antibody Avidity and Cross-Neutralization of Severe Acute Respiratory Syndrome Coronavirus 2 Variants by Hyperimmunized Transchromosomic Bovine-Derived Human Immunoglobulins for Treatment of Coronavirus Disease 2019. J. Infect. Dis. *226*, 655–663. https://doi.org/10.1093/infdis/jiac031.
46. Gilliland, T., Dunn, M., Liu, Y., Alcorn, M.D.H., Terada, Y., Vasilatos, S., Lundy, J., Li, R., Nambulli, S., Larson, D., et al. (2023). Transchromosomic bovine-derived anti-SARS-CoV-2 polyclonal human antibodies protects hACE2 transgenic hamsters against multiple variants. iScience *26*, 107764. https://doi.org/10.1016/j.isci.2023.107764.
47. Taiwo, B.O., Chew, K.W., Moser, C., Wohl, D.A., Daar, E.S., Li, J.Z., Greninger, A.L., Bausch, C., Luke, T., Hoover, K., et al. (2023). Phase 2 Safety and Antiviral Activity of SAB-185, a Novel Polyclonal Antibody Therapy for Nonhospitalized Adults With COVID-19. J. Infect. Dis. *228*, 133–142. https://doi.org/10.1093/infdis/jiad013.
48. Saied, A.A., Nascimento, M.S.L., do Nascimento Rangel, A.H., Skowron, K., Grudlewska-Buda, K., Dhama, K., Shah, J., Abdeen, A., El-Mayet, F.S., Ahmed, H., and Metwally, A.A. (2022). Transchromosomic bovines-derived broadly neutralizing antibodies as potent biotherapeutics to counter important emerging viral pathogens with a special focus on SARS-CoV-2, MERS-CoV, Ebola, Zika, HIV-1, and influenza A virus. J. Med. Virol. *94*, 4599–4610. https://doi.org/10.1002/jmv.27907.
49. Joyce, M.G., Chen, W.H., Sankhala, R.S., Hajduczki, A., Thomas, P.V., Choe, M., Martinez, E.J., Chang, W.C., Peterson, C.E., Morrison, E.B., et al. (2021). SARS-CoV-2 ferritin nanoparticle vaccines elicit broad SARS coronavirus immunogenicity. Cell Rep. *37*, 110143. https://doi.org/10.1016/j.celrep.2021.110143.
50. Joyce, M.G., King, H.A.D., Elakhal-Naouar, I., Ahmed, A., Peachman, K.K., Macedo Cincotta, C., Subra, C., Chen, R.E., Thomas, P.V., Chen, W.H., et al. (2022). A SARS-CoV-2 ferritin nanoparticle vaccine elicits protective immune responses in nonhuman primates. Sci. Transl. Med. *14*, eabi5735. https://doi.org/10.1126/scitranslmed.abi5735.
51. King, H.A.D., Joyce, M.G., Lakhal-Naouar, I., Ahmed, A., Cincotta, C.M., Subra, C., Peachman, K.K., Hack, H.R., Chen, R.E., Thomas, P.V., et al. (2021). Efficacy and breadth of adjuvanted SARS-CoV-2 receptor-binding domain nanoparticle vaccine in macaques. Proc. Natl. Acad. Sci. USA *118*, e2106433118. https://doi.org/10.1073/pnas.2106433118.
52. Wuertz, K.M., Barkei, E.K., Chen, W.H., Martinez, E.J., Lakhal-Naouar, I., Jagodzinski, L.L., Paquin-Proulx, D., Gromowski, G.D., Swafford, I., Ganesh, A., et al. (2021). A SARS-CoV-2 spike ferritin nanoparticle vaccine protects hamsters against Alpha and Beta virus variant challenge. NPJ Vaccines *6*, 129. https://doi.org/10.1038/s41541-021-00392-7.
53. Shrivastava, S., Carmen, J.M., Lu, Z., Basu, S., Sankhala, R.S., Chen, W.H., Nguyen, P., Chang, W.C., King, J., Corbitt, C., et al. (2023). SARS-CoV-2 spike-ferritin-nanoparticle adjuvanted with ALFQ induces long-lived plasma cells and cross-neutralizing antibodies. NPJ Vaccines *8*, 43. https://doi.org/10.1038/s41541-023-00638-6.
54. Johnston, S.C., Ricks, K.M., Lakhal-Naouar, I., Jay, A., Subra, C., Raymond, J.L., King, H.A.D., Rossi, F., Clements, T.L., Fetterer, D., et al. (2022). A SARS-CoV-2 Spike Ferritin Nanoparticle Vaccine Is Protective and Promotes a Strong Immunological Response in the Cynomolgus Macaque Coronavirus Disease 2019 (COVID-19) Model. Vaccines *10*, 717. https://doi.org/10.3390/vaccines10050717.
55. Ober Shepherd, B.L., Scott, P.T., Hutter, J.N., Lee, C., McCauley, M.D., Guzman, I., Bryant, C., McGuire, S., Kennedy, J., Chen, W.H., et al. (2024). SARS-CoV-2 recombinant spike ferritin nanoparticle vaccine adjuvanted with Army Liposome Formulation containing monophosphoryl lipid A and QS-21: a phase 1, randomised, double-blind, placebo-controlled, first-in-human clinical trial. Lancet. Microbe *5*, e581–e593. https://doi.org/10.1016/S2666-5247(23)00410-X.
56. Dussupt, V., Sankhala, R.S., Gromowski, G.D., Donofrio, G., De La Barrera, R.A., Larocca, R.A., Zaky, W., Mendez-Rivera, L., Choe, M., Davidson, E., et al. (2020). Potent Zika and dengue cross-neutralizing antibodies induced by Zika vaccination in a dengue-experienced donor. Nat. Med. *26*, 228–235. https://doi.org/10.1038/s41591-019-0746-2.
57. Scheaffer, S.M., Lee, D., Whitener, B., Ying, B., Wu, K., Liang, C.Y., Jani, H., Martin, P., Amato, N.J., Avena, L.E., et al. (2023). Bivalent SARS-CoV-2 mRNA vaccines increase breadth of neutralization and protect against the BA.5 Omicron variant in mice. Nat. Med. *29*, 247–257. https://doi.org/10.1038/s41591-022-02092-8.
58. Davis-Gardner, M.E., Lai, L., Wali, B., Samaha, H., Solis, D., Lee, M., Porter-Morrison, A., Hentenaar, I.T., Yamamoto, F., Godbole, S., et al. (2023). Neutralization against BA.2.75.2, BQ.1.1, and XBB from mRNA Bivalent Booster. N. Engl. J. Med. *388*, 183–185. https://doi.org/10.1056/NEJMc2214293.

59. Kurhade, C., Zou, J., Xia, H., Liu, M., Chang, H.C., Ren, P., Xie, X., and Shi, P.Y. (2023). Low neutralization of SARS-CoV-2 Omicron BA.2.75.2, BQ.1.1, and XBB.1 by parental mRNA vaccine or a BA.5-bivalent booster. Nat. Med. *29*, 344–347. https://doi.org/10.1038/s41591-022-02162-x.
60. Wang, Q., Iketani, S., Li, Z., Liu, L., Guo, Y., Huang, Y., Bowen, A.D., Liu, M., Wang, M., Yu, J., et al. (2023). Alarming antibody evasion properties of rising SARS-CoV-2 BQ and XBB subvariants. Cell *186*, 279–286.e8. https://doi.org/10.1016/j.cell.2022.12.018.
61. Magnus, C.L., Hiergeist, A., Schuster, P., Rohrhofer, A., Medenbach, J., Gessner, A., Peterhoff, D., and Schmidt, B. (2022). Targeted escape of SARS-CoV-2 in vitro from monoclonal antibody S309, the precursor of sotrovimab. Front. Immunol. *13*, 966236. https://doi.org/10.3389/fimmu.2022.966236.
62. Focosi, D., Quiroga, R., McConnell, S., Johnson, M.C., and Casadevall, A. (2023). Convergent Evolution in SARS-CoV-2 Spike Creates a Variant Soup from Which New COVID-19 Waves Emerge. Int. J. Mol. Sci. *24*, 2264. https://doi.org/10.3390/ijms24032264.
63. Cox, M., Peacock, T.P., Harvey, W.T., Hughes, J., Wright, D.W., COVID-19 Genomics UK COG-UK Consortium, Willett, B.J., Thomson, E., Gupta, R.K., Peacock, S.J., et al. (2023). SARS-CoV-2 variant evasion of monoclonal antibodies based on in vitro studies. Nat. Rev. Microbiol. *21*, 112–124. https://doi.org/10.1038/s41579-022-00809-7.
64. Rappazzo, C.G., Tse, L.V., Kaku, C.I., Wrapp, D., Sakharkar, M., Huang, D., Deveau, L.M., Yockachonis, T.J., Herbert, A.S., Battles, M.B., et al. (2021). Broad and potent activity against SARS-like viruses by an engineered human monoclonal antibody. Science *371*, 823–829. https://doi.org/10.1126/science.abf4830.
65. Yu, J., Thomas, P.V., McMahan, K., Jacob-Dolan, C., Liu, J., He, X., Hope, D., Martinez, E.J., Chen, W.H., Sciacca, M., et al. (2022). Protection against SARS-CoV-2 Omicron BA.1 variant challenge in macaques by prime-boost vaccination with Ad26.COV2.S and SpFN. Sci. Adv. *8*, eade4433. https://doi.org/10.1126/sciadv.ade4433.
66. Sankhala, R.S., Lal, K.G., Jensen, J.L., Dussupt, V., Mendez-Rivera, L., Bai, H., Wieczorek, L., Mayer, S.V., Zemil, M., Wagner, D.A., et al. (2024). Diverse array of neutralizing antibodies elicited upon Spike Ferritin Nanoparticle vaccination in rhesus macaques. Nat. Commun. *15*, 200. https://doi.org/10.1038/s41467-023-44265-0.
67. Navas, C., Manso, T., Martins, F., Minto, L., Moreira, R., Minozzo, J., Antunes, B., Vale, A., McDaniel, J.R., Ippolito, G.C., and Felicori, L.F. (2022). The major role of junctional diversity in the horse antibody repertoire. Mol. Immunol. *151*, 231–241. https://doi.org/10.1016/j.molimm.2022.09.011.
68. van der Straten, K., Guerra, D., van Gils, M.J., Bontjer, I., Caniels, T.G., van Willigen, H.D.G., Wynberg, E., Poniman, M., Burger, J.A., Bouhuijs, J.H., et al. (2022). Antigenic cartography using sera from sequence-confirmed SARS-CoV-2 variants of concern infections reveals antigenic divergence of Omicron. Immunity *55*, 1725–1731.e4. https://doi.org/10.1016/j.immuni.2022.07.018.
69. Wilks, S.H., Mühlemann, B., Shen, X., Türeli, S., LeGresley, E.B., Netzl, A., Caniza, M.A., Chacaltana-Huarcaya, J.N., Corman, V.M., Daniell, X., et al. (2023). Mapping SARS-CoV-2 antigenic relationships and serological responses. Science *382*, eadj0070. https://doi.org/10.1126/science.adj0070.
70. Lopardo, G., Belloso, W.H., Nannini, E., Colonna, M., Sanguineti, S., Zylberman, V., Muñoz, L., Dobarro, M., Lebersztein, G., Farina, J., et al. (2021). RBD-specific polyclonal F(ab)(2) fragments of equine antibodies in patients with moderate to severe COVID-19 disease: A randomized, multicenter, double-blind, placebo-controlled, adaptive phase 2/3 clinical trial. EClinicalMedicine *34*, 100843. https://doi.org/10.1016/j.eclinm.2021.100843.
71. Kimber, C., Valk, S.J., Chai, K.L., Piechotta, V., Iannizzi, C., Monsef, I., Wood, E.M., Lamikanra, A.A., Roberts, D.J., McQuilten, Z., et al. (2023). Hyperimmune immunoglobulin for people with COVID-19. Cochrane Database Syst. Rev. *1*, CD015167. https://doi.org/10.1002/14651858.CD015167.pub2.
72. Malyala, P., and Singh, M. (2008). Endotoxin limits in formulations for preclinical research. J. Pharmacol. Sci. (Tokyo, Jpn.) *97*, 2041–2044. https://doi.org/10.1002/jps.21152.
73. Wrapp, D., Wang, N., Corbett, K.S., Goldsmith, J.A., Hsieh, C.L., Abiona, O., Graham, B.S., and McLellan, J.S. (2020). Cryo-EM structure of the 2019-nCoV spike in the prefusion conformation. Science *367*, 1260–1263.
74. Joyce, M.G., Sankhala, R.S., Chen, W.H., Choe, M., Bai, H., Hajduczki, A., Yan, L., Sterling, S.L., Peterson, C.E., Green, E.C., and Smith, C. (2020). A Cryptic Site of Vulnerability on the Receptor Binding Domain of the SARS-CoV-2 Spike Glycoprotein. Preprint at BioRxiv. https://doi.org/10.1101/2020.03.15.992883.
75. Motulsky, H.J., and Brown, R.E. (2006). Detecting outliers when fitting data with nonlinear regression - a new method based on robust nonlinear regression and the false discovery rate. BMC Bioinformatics *7*, 123. https://doi.org/10.1186/1471-2105-7-123.
76. Martinez, E.J., Chang, W.C., Chen, W.H., Hajduczki, A., Thomas, P.V., Jensen, J.L., Choe, M., Sankhala, R.S., Peterson, C.E., Rees, P.A., and Kimner, J. (2024). SARS-CoV-2 ferritin nanoparticle vaccines produce hyperimmune equine sera with broad sarbecovirus activity. iScience.

STAR★METHODS

KEY RESOURCES TABLE

REAGENT or RESOURCE	SOURCE	IDENTIFIER
Bacterial and virus strains		
Stbl3 competent cells	ThermoFisher Scientific	Cat# C737303
Top10 competent cells	ThermoFisher Scientific	Cat# C404010
SARS-CoV-2/human/USA/WA-CDC-WA1/2020	CDC	GenBank: MN985325.1
Chemicals, peptides, and recombinant proteins		
3,5,3′5′-tetramethylbenzidine (TMB)	KPL	Cat# 5150-0021
SARS-CoV-1 RBD (Urbani) protein	This manuscript	N/A
SARS-CoV-2 S-2P (WA-1) protein	Wrapp et al.[72]	N/A
SARS-CoV-2 S-RBD (WA-1) protein	Joyce et al.[73]	N/A
SARS-CoV-2 (Alpha) RBD protein	This manuscript	N/A
SARS-CoV-2 (Beta) RBD protein	This manuscript	N/A
SARS-CoV-2 (Delta) RBD protein	This manuscript	N/A
SARS-CoV-2 (BA.1) RBD protein	This manuscript	N/A
SARS-CoV-2 (BA.2) RBD protein	This manuscript	N/A
SARS-CoV-2 (BA.4/5) RBD protein	This manuscript	N/A
SARS-CoV-2 (XBB.1.5) RBD protein	This manuscript	N/A
RaTG13 RBD protein	This manuscript	N/A
SHC014 RBD protein	This manuscript	N/A
WIV1 RBD protein	This manuscript	N/A
BANAL-20-247 RBD protein	This manuscript	NCBI accession MZ937004
Shaanxi2011 RBD protein	This manuscript	JX993987
ZXC21 RBD protein	This manuscript	MG772934
BM48-31 RBD protein	This manuscript	NC_014470
Khosta-2 RBD protein	This manuscript	MZ190138
RhGB01 RBD protein	This manuscript	MW719567
BtKY72 RBD protein	This manuscript	KY352407
RaTG15 RBD protein	This manuscript; Martinez et al.[74]	https://ngdc.cncb.ac.cn/gwh/Assembly/18716/show GWHBAUP01000000
RsYN04 RBD protein	This manuscript	MZ081380
Imidazole	ThermoFisher Scientific	Cat# AC122020050
PBS	ThermoFisher Scientific	Cat# 10010023
Bovine serum albumin	Sigma-Aldrich	Cat# A8327
HIS1K sensors	ForteBio	Cat# 18-5120
FreeStyle 293 Expression Medium	GIBCO	Cat# 12338002
OPTI-MEM, Reduced Serum Medium	ThermoFisher Scientific	Cat# 11058021
Methyl-α -D mannopyranoside	Sigma Aldrich	Cat# 617-04-9
DPBS	ThermoFisher Scientific	Cat# 14-190-235
FCA	Sigma Aldrich	F5881
IFA	Sigma Aldrich	F5506

(*Continued on next page*)

Continued

REAGENT or RESOURCE	SOURCE	IDENTIFIER
Glycerol	ThermoFisher Scientific	Cat# BP229-1
SpFN (pCoV1B-06: S2P(1–1158)op1-del-Ferritin protein)	This manuscript	N/A
pCoV131 (aka RFN): His8-3C-RBD-Y453R/ L517N/L518K/H519S-Ferritin protein	This manuscript	N/A
Critical commercial assays		
Bright-Glo Luciferase Assay System	Promega	Cat# E2610
Experimental models: Cell lines		
Freestyle 293F cells	ThermoFisher Scientific	Cat# R7007
Expi293F cells	ThermoFisher Scientific	Cat# A14635
hACE2-expressing HEK293cells	Integral Molecular	N/A
Experimental models: Organisms/strains		
Horses (female)	BSV Biosciences	N/A
Mus musculus, strain B6.Cg-Tg(K18-ACE2)2Prlmn/J	Jackson Laboratories	JAX stock #034860
Recombinant DNA		
SARS-CoV-1 RBD (Urbani)	This manuscript	N/A
SARS-CoV-2 S-2P (WA-1)	Wrapp et al.[72]	N/A
SARS-CoV-2 S-RBD (WA-1)	Joyce et al.[73]	N/A
SARS-CoV-2 (Alpha) RBD	This manuscript	N/A
SARS-CoV-2 (Beta) RBD	This manuscript	N/A
SARS-CoV-2 (Delta) RBD	This manuscript	N/A
SARS-CoV-2 (BA.1) RBD	This manuscript	N/A
SARS-CoV-2 (BA.2) RBD	This manuscript	N/A
SARS-CoV-2 (BA.4/5) RBD	This manuscript	N/A
SARS-CoV-2 (XBB.1.5) RBD	This manuscript	N/A
RaTG13 RBD	This manuscript	N/A
SHC014 RBD	This manuscript	N/A
WIV1 RBD	This manuscript	N/A
BANAL-20-247 RBD	This manuscript	NCBI accession MZ937004
Shaanxi2011 RBD	This manuscript	JX993987
ZXC21 RBD	This manuscript	MG772934
BM48-31 RBD	This manuscript	NC_014470
Khosta-2 RBD	This manuscript	MZ190138
RhGB01 RBD	This manuscript	MW719567
BtKY72 RBD	This manuscript	KY352407
RaTG15 RBD	This manuscript; Martinez et al.[74]	https://ngdc.cncb.ac.cn/gwh/Assembly/18716/show GWHBAUP01000000
RsYN04 RBD	This manuscript	MZ081380
Software and algorithms		
Octet Data Analysis software	FortéBio	v11.1
GraphPad Prism	Motulsky and Brown[75]	V8.0
PyMol	Schrödinger	V2.3.2
SnapGene	Insightful Science	https://www.snapgene.com/

(*Continued on next page*)

Continued

REAGENT or RESOURCE	SOURCE	IDENTIFIER
Other		
Strep-Tactin Superflow resin	IBA Lifesciences	Cat# 2-1206-010
Pierce™ Protein A Agarose	ThermoFisher Scientific	Cat# 20334
Superdex 200 increase 10/300 GL	Cytiva	Cat# 28990944
Galanthus Nivalis Lectin (GNL), Agarose bound	Vector Labs	Cat# AL-1243-5
NiNTA Resin	Thermo Fisher Scientific	Cat# 88221

EXPERIMENTAL MODEL AND STUDY PARTICIPANT DETAILS

Cell lines

Expi293F cells (Thermo Fisher Scientific) were maintained in Expi293 expression medium (Thermo Fisher Scientific) in a 37°C shaker supplied with 8% CO_2 and 80% humidity.

Horse strain

Female horses (ponies) weighing between 200 and 250 kg aged 5–6 years were quarantined for 21 days before immunization. At the end of the quarantine period, blood was drawn and tested against the antigen for reactivity in ELISA. A part of the plasma was aliquoted and stored at −20°C, which served as negative control throughout the study. A total of 12 animals were immunized subcutaneously with 2 mL of vaccine emulsified with FCA for the primary dose and FIA for the subsequent boosters. The animals were divided into two groups of 6 animals each, one group receiving pCoV1B-06-PL vaccine and the other receiving pCoV131 vaccine. The vaccines were diluted in PBS to a required concentration and emulsified in equal volume of either Freund's Complete Adjuvant or Freund's Incomplete Adjuvant for immunization. The animals were maintained on a high-protein diet with water provided *ad libitum*. The blood was collected 7–10 days after the administration of vaccine and the plasma was separated, aliquoted and stored at −20°C until testing.

Mouse strain

Female and male hACE2 K18 Transgenic mice aged 6- to 8-week were obtained from Jackson Laboratory (Bar Harbor, ME). All mouse experiments were conducted in compliance with the Animal Welfare Act, and other federal statutes and regulations relating to animals and experiments involving animals and adhered to the principles stated in the Guide for the Care and Use of Laboratory Animals, NRC Publication, 1996 edition.

All infection experiments were done in animal biosafety level 3 (BSL-3) facilities at the Trudeau Institute and approved by the Institutional Animal Care and Use Committee of the Trudeau Institute.

METHOD DETAILS

Protein production

The SARS-CoV-2 Spike Ferritin Nanoparticle (SpFN) or the RBD-Ferritin Nanoparticle (RFN) protein immunogens were prepared as previously described.[49] SARS-CoV-2 constructs were derived from the Wuhan-Hu-1 strain genome sequence (GenBank MN9089473), to include the RBD subunit (residues 331–527) or spike prefusion ectodomain (residues 12 to 1158) linked to *Helicobacter pylori* ferritin. Constructs were expressed using the pCMVR vector and the RFN construct was modified to incorporate an N-terminal hexahistidine tag (His) for purification. Recombinant RBD proteins were expressed using the pCMVR vector in Freestyle cells at 37°C and included the RBD subunit (residues 331–527) from the following viruses with corresponding accession numbers: Alpha: MZ344997.1; Beta: MW598419.1; Delta: MZ009823.1; Omicron BA.1: OL672836.1; Omicron BA.2: OM371884.1; OmicronBA.4/5: ON249995.1; RaTG13: MN996532; SARS-CoV-1: AY278741.1; SHC014: KC881005; WIV1: KF367457; BANAL20-247: MZ937004; Shaanxii 2011: JX993987; ZXC21: MG772934; BM48-31: NC_014470; Khosta-2: MZ190138; RhGB01: MW719567; BtKY72: KY352407; RaTG15: GWHBAUP01000000; RsYN04: MZ081380.

SpFN and RFN were produced in Expi293 mammalian cells at 34°C (Thermo Fisher Scientific) and purified by *Galanthus nivalis* lectin or nickel-nitrilotriacetic acid (NiNTA) based affinity chromatography and Superdex200 size exclusion chromatography. The purified immunogens were filter-sterilized using Ultrafree-MC GV Centrifugal Filters (0.22μm filter). The resulting material was tested for endotoxin to ensure levels were below 5 EU/kg/h[76] if it was to be used as an immunogen. The His-tag on the RFN molecule was not enzymatically removed for the immunization experiments. Purified immunogens were formulated in PBS with 5% glycerol at 1 mg/mL and flash-frozen in liquid nitrogen and stored at −80°C. In addition, the immunogens were assessed for antigenicity using a set of neutralizing antibodies, and non-neutralizing antibodies to ensure the antigenic profile was consistent with immunogens previously assessed in mice and non-human primates, and to ensure minimal batch-to-batch variation. The structure of the nanoparticles was assessed by visualization using negative-stain electron microscopy (EM) to ensure (i) nanoparticle formation, and (ii) spike or RBD structure visible on the nanoparticle surface and equivalent appearance to the previously assessed nanoparticle immunogens.

Animal groups and immunization/assay schedule

Horses (n = 3/group) were immunized subcutaneously with either 150 μg or 500 μg of SpFN or RFN. Immunogens were administered in a 2.0 mL dose formulated in Complete Freund's Adjuvant (CFA) for the prime dose and Incomplete Freund's Adjuvant (IFA) for the boost doses. Immunizations were administered with two schedules as shown in Figure 1 with animals immunized three times with schedule 1 (day 0, day 21, and day 42) or schedule 2 (day 0, day 28, and day 56). Blood was collected regularly at 1-week or 2-week post immunization. Sera was stored at −80°C until analysis. Antibody binding and neutralization were analyzed by ELISA, Octet Biolayer Interferometry, and pseudovirus neutralization assay.

Purification of IgG from equine sera

In vitro binding studies

Sera from selected samples were further processed to obtain purified IgGs. Serum vials stored at −80°C were thawed at 4°C. 4 mL Protein A resin (rProtein A Sepharose Fast Flow, Cytiva) and 4 mL Protein G resin (Protein G Sepharose 4 Fast Flow, Cytiva) were mixed together and equilibrated with ∼85 mL PBS. This mixed resin was then resuspended with 13 mL PBS and serum was added and allowed to incubate on a rotating inverter at 4°C for approximately 90 min. These mixtures were loaded into chromatography columns at 4°C; the flowthroughs were reloaded 4x. These columns were then washed at 4°C with 50 mL PBS, then eluted at room temperature in 40 mL fractions using IgG elution buffer (Pierce, 0.1M glycine-HCl pH 2.8) into tubes containing 2 mL 2M Tris pH 8.0, inverting to mix upon collection. Fractions containing IgG as confirmed by SDS-PAGE were dialyzed (10K MWCO) into PBS pH 7.4 at 4°C followed by filter-sterilization at 0.22 μm.

In vivo protection study

Equine serum/plasma samples (total 9mL pooled sera for either SpFN or RFN groups) were diluted with PBS (volume ratio 1:2, sera: PBS) and passed through 2.5 mL Immobilized Protein A Sepharose pre-equilibrated with PBS by gravity flow at 22°C (RT). The Protein A resin was then washed with 3x 5mL PBS by gravity flow at RT. Bound IgG was eluted from the column with 2.5mL per fraction (10mL total) using ImmunoPure (G) IgG Elution Buffer (Pierce). The pooled fraction was mixed with 1 mL of 1M Tris pH 8.5 and then dialyzed against 4L PBS overnight at 4°C. After O/N dialysis the eluates were concentrated to OD280 = 30. The purified IgG was assessed for activity by biolayer interferometry. The Omicron XBB.1.5 RBD molecule (30 μg/mL diluted in PBS) was immobilized to the anti-His-tag biosensors (HIS1K biosensors with a conjugated Penta-His antibody (FortéBio). Binding to the purified polyclonal IgG (100-fold dilution) was allowed to associate for 180 s. The binding response to the XBB.1.5 RBD at 180 s for the SpFN sample was 1.22 nm and for RFN was 1.80 nm.

ELISA

The 96-well ELISA plates (Immuno Module, Nunc, Thermo Fisher Scientific) were coated with 250 ng/well of recombinant RBD protein (Sino Biological Cat # RBD40592) or spike protein (Genscript Cat #Z03481), prepared in 50 mM carbonate buffer, pH 9.6 and incubated overnight at 2°C–8°C. Plates were blocked with PBS containing 0.1% Tween 20 and 2% skimmed milk, pH 7.2 (blocking buffer) and incubated at 37°C for 1 h. The plates were then washed with PBS containing 0.05% Tween 20, pH 7.2 (wash buffer). To determine the titers, the serum samples collected from horses at different stages during the immunization protocol were serially diluted in blocking buffer, starting at 1:200 dilution. The diluted samples were dispensed into wells coated with either RBD or spike protein. The plates were incubated for 1 h at room temperature, followed by 5 washes in wash buffer. Horseradish peroxidase (HRP)-conjugated goat anti-horse IgG (Bethyl Catalog # A70-106P) was added at a 1:20,000 dilution and incubated at 25°C for 1 h. The plates were then washed 5 times with wash buffer. For color development, TMB substrate (BioRad Catalog #1721067) was added and incubated for 10 min. The reaction was terminated by addition of stop solution (2N H_2SO_4). Absorbance was measured at 450 nm using an ELISA reader. Titer is defined as the antibody dilution at which the sample OD_{450} is twice that of the OD_{450} of negative control.

To test polyclonal IgG binding, 96-well Immulon "U" Bottom plates were coated with 5 μg/mL of RBD antigens in PBS. Plates were incubated at room temperature (RT) for 2 h and blocked with blocking buffer (Dulbecco's PBS containing 0.2% bovine serum albumin, pH 7.4), at room RT for 30 min, followed by 3 times washing with wash buffer (Dulbecco's PBS containing 0.05% Tween 20, pH 7.4). Polyclonal IgG samples were serially diluted 3-fold, starting at 0.43 mg/mL, in sample buffer (Dulbecco's PBS containing 0.2% bovine serum albumin and 0.05% Tween 20, pH 7.4), added to duplicate wells and the plates were incubated for 1 h at RT, followed by 3 washes in wash buffer. Horseradish peroxidase (HRP)-conjugated rabbit anti-horse IgG (Sigma, catalog number SAB3700152-1.5ML) was added at a 1:1,000 dilution and incubated at RT for 30 min. Plates were then washed 3 times with wash buffer and once with PBS. For color development, the substrate mixture from TMB Substrate set (Biolegend) was added and incubated for 11 min, before the addition of the Stop Solution for TMB Substrate (Biolegend). Absorbance (A) was measured at 450 nm using an ELISA reader Spectramax (Molecular Devices, San Jose, CA).

RBD binding, and DPP4 competition by biolayer interferometry

All biosensors were hydrated in PBS prior to use. All assay steps were performed at 30°C with agitation set at 1,000 rpm using an Octet 96red instrument (FortéBio). For binding assays, baseline equilibration of the anti-His-tag biosensors (HIS1K biosensors with a conjugated Penta-His antibody (FortéBio) was carried out using assay buffer (PBS) for 15 s, prior to His-tagged RBD (30 μg/mL diluted in PBS) loading for 120 s. After briefly dipping in assay buffer (15 s), the biosensors were dipped in the horse sera samples (100-fold dilution) to associate for 180 s, followed by dipping in assay buffer for 60 s to dissociate. The binding response (nm) at 180 s was recorded for each sample.

For DPP4-competition assays, baseline equilibration of the anti-His-tag biosensors (HIS1K biosensors with a conjugated Penta-His antibody (FortéBio) was carried out using assay buffer (PBS) for 30 s, prior to His-tagged RBD (30 μg/mL diluted in PBS) loading for 120 s followed by association of purified polyclonal (pAb) horse IgG samples (12 mg/mL diluted to 0.6 mg/mL) for 180 s. The biosensors were dipped in assay buffer for 30 s to wash off unbound pAb IgG and then dipped in DPP4-Fc recombinant protein (30 μg/mL diluted in PBS) for 120 s. The response at the end of these steps (nm) was recorded for each sample. PBS control was used as baseline for 100 percent DPP4 binding, or no percent competition, and percent inhibition (PI) of DPP4 binding to the RBD by pAb IgG was determined using the equation: PI = 100 − ((DPP4 binding in the presence of pAb IgG/DPP4 binding in PBS alone) × 100).

SARS-CoV-2 WA-1 and VOCs and SARS-CoV-1 pseudovirus neutralization assay

The spike sequences for SARS-CoV-2 WA-1, Alpha, Beta, Delta, Omicron BA.1, Omicron BA.5, Omicron XBB.1.5, and SARS-CoV-1 were codon optimized and modified to remove an 18 amino acid endoplasmic reticulum retention signal in the cytoplasmic tail in the case of SARS-CoV-2, and a 28 amino acid deletion in the cytoplasmic tail in the case of SARS-CoV-1. These cytoplasmic tail deletions increased spike incorporation into pseudovirions and improved infectivity titers. SARS-CoV-2 pseudoviruses (PSV) were produced by co-transfection of a WA-1 SARS-CoV-2 (GenBank accession number: MN908947.3) spike protein-expressing plasmid (pcDNA3.4) and an HIV-1 (pNL4-3.Luc.R-E−, NIH HIV Reagent Program, Catalog number 3418) backbone in HEK293T/17 cells. PSV infectivity and neutralization titers were determined using ACE2-expressing HEK293 target cells (Integral Molecular) in a semi-automated assay format using robotic liquid handling (Biomek NXp Beckman Coulter). Virions pseudotyped with the vesicular stomatitis virus (VSV) G protein were used as a non-specific control. Test sera were diluted to 1:40 in growth medium; 10% FBS, 2.5% HEPES, 0.5% Gentamicin, 0.1% Puromycin in Dulbecco's Modified Eagle Medium (DMEM), and serially diluted; then 25 μL/well was added to a white 96-well plate. An equal volume of diluted PSV was added to each well and plates were incubated for 1 h at 37°C. HEK293 target cells were added to each well (40,000 cells/well) and plates were incubated for an additional 48 h. Relative light units (RLU) were measured with the EnVision Multimode Plate Reader (PerkinElmer, Waltham, MA) using the Bright-Glo Luciferase Assay System (Promega, Madison, WI). Neutralization dose-response curves were fitted by nonlinear regression using the LabKey Server. Final titers are reported as the reciprocal of the dilution of serum necessary to achieve 50% (ID_{50}, 50% inhibitory dose).

Contour-phylogenetic mapping

Phylogenetic analysis of betacoronavirus receptor binding domain sequence using Molecular Evolutionary Genetics Analysis (MEGA) 11.0.10 was carried out as follows. The ClustalW algorithm with default settings was used to align protein sequences corresponding to the receptor binding domain, residues 331–527 of SARS-CoV-2 WA-1 spike (GenBank ID: QHO60594.1) from SARS-CoV-2 Alpha (GenBank ID: MZ344997.1), Beta (GenBank ID: MW598419.1), Delta (GenBank ID: MZ009823.1), BA.1 (GenBank ID: OL672836.1), BA.2 (GenBank ID: OM371884.1), BA.2.12.1 (GenBank ID: OM958567.1), BA.4/5 (GenBank ID: ON249995.1), BA.2.75 (GenBank ID: ON990685.1), SARS-CoV-1 Urbani (GenBank ID: AY278741.1), SARS-CoV-1 Frankfurt (GenBank ID: BAE93401.1), BM48-31 (GenBank ID: NC_014470), RsSHC014 (GenBank ID: KC881005), WIV1 (GenBank ID: KF367457), ZXC21 (GenBank ID: MG772934), RaTG13 (GenBank ID: MN996532), BANAL 20–247 (GenBank ID: MZ937004), Rf4092 (GenBank ID: KY417145), Shaanxi 2011 (GenBank ID: JX993987), HeB2013 (GenBank ID: KJ473812), Rp3 (GenBank ID: DQ071615), Rs_672 (GenBank ID: FJ588686), RsYN04 (GenBank ID: MZ081380), Khosta-2 (GenBank ID: MZ190138), BtKY72 (GenBank ID: KY352407), RaTG15_Ra7909 (CNCB NGDC Accession No. GWHBAUP01000000), HKU3-1 (GenBank ID: DQ022305), RhGB01 (GenBank ID: MW719567), Pangolin-GX (GenBank ID: QIA48623.1), PCoV_GX-P5L (GenBank ID: QIA48632.1), PCoV_GX-P2V (GenBank ID: QIQ54048.1), Civet-SARS-CoV-007/2004 (GenBank ID: AAU04646.1), MERS England1 (GenBank ID: YP_007188579), MERS EMC/2012 (GenBank ID: AFS88936.1), Erinaceus/2012-174 (GenBank ID: NC_039207), Neoromicia/5038 (GenBank ID: MF593268), HKU4_SM3A (GenBank ID: MW218395), Ita1-205545-40 (GenBank ID: MG596802.1), Ita2-206645-63 (GenBank ID: MG596803.1), HKU5 (GenBank ID: NC_009020), OC43 (GenBank ID: AY585229.1), HKU-1 isolate N5 (GenBank ID: DQ339101.1), Hp_Zhejiang2013 (GenBank ID: KF636752), GCCDC1 (GenBank ID: KU762338.1), HKU93 (GenBank ID: EF065515), Rs4231 (GenBank ID: KY417146), Rs4084 (GenBank ID: KY417144), RmYN05_2020 (GenBank ID: MZ081376), RmYN08_2020 (GenBank ID: MZ081378), WIV16 (GenBank ID: KT444582), Rs3367 (GenBank ID: KC881006), Rs7327 (GenBank ID: ATO98218.1), RpYN06_2020 (GenBank ID: MZ081381), bat-SL-CoVZC45 (GenBank ID: AVP78031.1), RacCS203 (GenBank ID: MW251308), BANAL-20-116 (GenBank ID: MZ937002.1), BtRfBetaCoV_JL2012 (GenBank ID: KJ473811), BtRlBetaCoV_SC2018 (GenBank ID: MK211374), BtRsBetaCoV_HuB2013 (GenBank ID: KJ473814), Bat.YNLF_31C (GenBank ID: KP886808), Bat.YNLF_34C (GenBank ID: KP886809), BtCoV.273.2005 (GenBank ID: DQ648856), BtRsBetaCoV_YN2018D (GenBank ID: MK211378), RmYN07_2020 (GenBank ID: MZ081377), Cp/Yunnan2011 (GenBank ID: JX993988.1), RsYN03_2019 (GenBank ID: MZ081379), BtCoV.279.2005 (GenBank ID: DQ648857), BtRsBetaCoV_GX2013 (GenBank ID: KJ473815), BtRsBetaCoV_YN2013 (GenBank ID: KJ473816), RsYN09_2020 (GenBank ID: MZ081382), Khosta-1 (GenBank ID: MZ190137.1), BB9904/BGR/2008 (GenBank ID: KR559017.1), Rc-mk2 (GenBank ID: BDD37268.1), Rc-os20 (GenBank ID: BDD37258.1), Rc-o319 (GenBank ID: BCG66627.1), Rc-kw8 (GenBank ID: BDD37176.1). A maximum likelihood phylogenetic tree of these sequences was generated using a Jones-Taylor-Thornton model, the MEGA 11 default NJ/BioNJ Initial Tree method, and nearest-neighbor-interchange maximum likelihood heuristic. This analysis used a total of 304 positions and the 77 amino acid sequences noted above. Sequences where binding data was not collected were removed from the tree and branches were swapped manually to aid in contour visualization and label placement. The tree was exported into Inkscape and X and Y coordinates for the center of a circle placed at the end of each branch were recorded and matched to a Z coordinate representing serum BLI binding to the respective RBD for each timepoint and immunogen. A thin plate radial basis function (r^2*log(r)) within the scipy python package was used to interpolate and extrapolate Z coordinates between measured points on the phylogenetic tree to create an antigenic contour map displayed underneath

the phylogenetic tree. The Z value at each of the X,Y coordinates was checked to match the measured serum BLI binding and extrapolated values outside of the measured BLI binding range were truncated to 0 for the lowest value, and to the highest binding value for each plot.

K18-hACE2 transgenic mouse passive immunization and challenge

All research in this study involving animals was conducted in compliance with the Animal Welfare Act, and other federal statutes and regulations relating to animals and experiments involving animals and adhered to the principles stated in the Guide for the Care and Use of Laboratory Animals, NRC Publication, 1996 edition. The research protocol was approved by the Institutional Animal Care and Use Committee of the Trudeau Institute, protocol 20–007, and the USAMRDC Office of Research Protections, Animal Care and Use Review Office log number DM170728.e022. K18-hACE2 transgenic mice were obtained from Jackson Laboratories (Bar Harbor, ME). Mice were housed in the animal facility of the Trudeau Institute and cared for in accordance with local, state, federal, and institutional policies in a National Institutes of Health American Association for Accreditation of Laboratory Animal Care-accredited facility. Animals were maintained in IVC cages on negatively pressurized Allentown PNC racks that were HEPA filtered and directly vented though the building's exhaust system. The racks and animal rooms were negatively pressurized. Access to all facilities is controlled electronically by the buildings management systems and restricted to approved users only. The environment, temperature, and humidity, within the animal facility room were constantly monitored by the building management system. Temperatures were also monitored and recorded daily in individual animal rooms by animal care staff using electronic thermometers. All temperature set points were within The Guide recommended range of 68–79°F for mice. Acceptable Institutional daily fluctuations are between 67 and 74°F with a humidity range of 30–70%. Light cycles in all animal holding and procedure spaces are controlled on a 12/12 light/dark cycle.

For the passive immunization studies, one day prior to challenge, 200 μL of purified equine polyclonal IgG (OD280 = 30), or a control human IgG antibody MZ4 (400 μg) were injected into the intraperitoneal cavity of three groups of K18-hACE2 mice. The MZ4 human IgG1 antibody was prepared by transient transfection in 293F cells and purified by protein A affinity prior to storage at −80°C, as previously described.[56] Each animal study group consisted of 10 mice (5 female, 5 male), aged 6–10 weeks old. On study day 0, all mice were infected with 1.25×10^4 PFU of SARS-CoV-2 Omicron XBB.1.5 virus via intranasal instillation. The viral titer used for infection was previously determined to provide robust and reproducible infection, and consistent weight loss in this model. The day 2 timepoint for recovery and analysis of lung viral load was determined as the timepoint with peak lung viral loads using this challenge virus stock. All mice were monitored for clinical symptoms and body weight twice daily, every 12 h, from study day 1 to study day 14. Mice were euthanized if they displayed any signs of pain or distress as indicated by the failure to move after stimulation or presentation of inappetence, or if a mouse had >25% weight loss compared to their study day 0 body weight. Animals were assigned a clinical score as follows: 0: normal appearance and movement, 1: slightly ruffled fur, 2: slightly ruffled fur and reduced mobility, 3: slightly ruffled fur, reduced mobility, and rapid breathing, 4: slightly ruffled fur, reduced mobility, rapid breathing and hunched and huddled stance, and 5: found dead or euthanized due to weight loss or being moribund. Two days post-challenge, viral loads were measured by plaque assay in the bronchoalveolar lavage of 5 animals from each group.

QUANTIFICATION AND STATISTICAL ANALYSIS

Figure legends detail all quantification and statistical analyses, inclusive of animal numbers (n), and statistical tests. All statistical analyses were conducted using GraphPad Prism v9.4.0. Significant difference for each body weight measurement timepoint between each group compared to the antibody isotype control group, was assessed by t-test. Significant difference for each clinical score measurement timepoint between each group, compared to the antibody isotype control group, was assessed by t-test. BAL (PFU/mL) viral levels in the two study groups were compared for significance against the control group using a Kruskal-Wallis ANOVA test followed by post hoc Dunn's multiple comparison test.